Structure and Bonding, Vol. 112 (2004)
DOI 10.1007/b12224

# The Calculation of NMR Parameters in Transition Metal Complexes

Jochen Autschbach

Department of Chemistry, University at Buffalo, NY 14260–3000, USA
*E–mail: jochena@buffalo.edu*

## Contents

**Abstract** An overview is presented of the methodology and computations of nuclear shielding and spin–spin coupling constants of transition metal complexes. The presented material also includes an outline of relativistic approaches and their applications to heavy transition metals.

**Keywords** Density functional calculations Transition metal complexes NMR chemical shifts Nuclear spin–spin coupling constants Relativistic quantum chemistry

## 1 Introduction

It is fair to state that reasonably accurate computations of NMR parameters for transition metal complexes have only become feasible due to the enormous development of density functional theory (DFT) methods for chemical applications (along with powerful computer hardware) during the 1990s. This has perhaps two main reasons: a) the strong influence of electron correlation in particular for the 3d metals, which render Hartree-Fock calculations of NMR parameters often unreliable (with exceptions, see Sec. 4), and b) the large number of electrons and the need for a relativistic treatment for complexes of the 4d and 5d metals. Relativistic DFT methods have also only during the last decade become efficient and accurate enough for routine applications in transition metal chemistry. This has in turn allowed the subsequent development of relativistic NMR program codes.

The application of DFT methods to the computation of transition metal NMR has been reviewed in the past [1–4]. A short overview was recently prepared by Bühl [5]. NMR calculations on heavier transition metal complexes have further been discussed in reviews devoted to relativistic NMR methodology [6–9]. Thus, the present overview does not attempt to give a full coverage of the available literature, but to present a number of illustrative examples, the present status of such computations and their accuracy and limitations, along with a description of the underlying methodology. Because of the high importance of relativistic effects on NMR parameters, which is clearly represented in the available literature on DFT NMR computations of transition metal complexes, the reader will find that a substantial portion of this paper is devoted to this topic.

The methodological section is intended for readers who are not very familiar with the theoretical details. Accordingly, only part of the formalism is presented in form of equations. However, the general quantum mechanical concepts that allow the computation of NMR observables from first principles theory, as well as some important technical details, are outlined. Sections 2.2 to 2.9 might be skipped by readers who are not interested in methodological details, since the subsequent sections do not make excessive references to the methodology part.

The discussion of theory as well as computational results is restricted to closed–shell systems. An account of calculations of NMR parameters for paramagnetic systems can be found in Ref. 10. Further, most of the applications that will be discussed in Sec. 4 are not concerned with the calculation of vibrational corrections to NMR parameters [11]. Most methodolocial advances in this field have so far been tested on comparatively small molecules containing main group elements. Only recently, some work on this important topic with applications to transition metal complexes has appeared in the literature [12–14]. Another restriction of the scope of this paper is the focus on isotropic shielding and spin–spin coupling constants. The tensorial properties of nuclear shielding and spin–spin coupling are only very briefly mentioned and the reader is referred to Ref. 15, 16 for further details.

In the methodology part, atomic units with $e = 1, m_e = 1, h = 2\pi, 4\pi\varepsilon_0 = 1$, and the speed of light $c = 137.03599976(50)$ are employed. Thus prefactors containing $e, m_e, 4\pi\varepsilon_0$ and $\hbar = h/(2\pi)$

are often dropped, whereas the speed of light, $c$, is explicitly included. Equations referring to magnetic properties have been converted from SI to atomic units. The fine structure constant $\alpha$ is in atomic units equal to $c^{-1}$. The latter occurs in the equations indicating the relative magnitude of the hyperfine terms in the Hamiltonian as compared to relativistic corrections of $\mathcal{O}(c^{-2})$ and the nonrelativistic terms $\mathcal{O}(c^0)$.

## 2 Methodological aspects of NMR computations

### 2.1 Nuclear magnetic resonance

The presence of magnetic moments $\boldsymbol{\mu}_A, \boldsymbol{\mu}_B, \ldots$ of nuclei $A, B, \ldots$ in a molecule are responsible for the two observables of the NMR experiment that are most frequently utilized in chemical applications. They are physically observed in form of quantized energy differences $\Delta E$ that can be measured very precisely. These two observables are the nuclear shielding tensor $\boldsymbol{\sigma}_A$ for nucleus $A$ and the so-called indirect reduced coupling tensor $\mathsf{K}_{AB}$ for a pair of nuclei $A$, $B$. Both $\boldsymbol{\sigma}_A$ and $\mathsf{K}_{AB}$ are 2nd rank tensors that are defined via the phenomenological Hamiltonians

$$H^{\text{spin}} = -\boldsymbol{\mu}_A(1-\boldsymbol{\sigma}_A)\mathbf{B}^{\text{ext}} \tag{1a}$$

for the shielding tensor and

$$H^{\text{spin}} = \boldsymbol{\mu}_A \mathsf{K}_{AB} \boldsymbol{\mu}_B \tag{1b}$$

for the spin–spin coupling. $\mathbf{B}^{\text{ext}}$ is the external magnetic field. Equations (1a,1b) do not contain any electronic degrees of freedom. The external field as well as the magnetic moments of the nuclei are fixed, known quantities which are experimentally determined, not quantum operators that act on electronic variables. $\boldsymbol{\mu}_A$ is related to the spin $\mathbf{I}_A$ of nucleus $A$ by

$$\boldsymbol{\mu}_A = \hbar \gamma_A \mathbf{I}_A \quad , \tag{2}$$

with $\gamma_A$ being the magneto-gyric ratio of $A$. The $\gamma$'s enter the relation between the reduced coupling tensor (in SI units of $\mathrm{T}^2\mathrm{J}^{-1}$) and the experimentally determined $\mathsf{J}$–tensor (in units of Hz):

$$\mathsf{J}_{AB} = \frac{\hbar}{2\pi}\gamma_A\gamma_B\mathsf{K}_{AB} \quad . \tag{3}$$

The rotational averages of the shielding and coupling tensors are the most important experimentally determined parameters. They are given by 1/3 of the trace (sum of diagonal elements) of the respective tensors and will be denoted with $\sigma_A$ or $\sigma(A)$ (isotropic shielding constant) and $K_{AB}$ or $K(A–B)$ ( reduced spin–spin coupling constant, similar for $J$) in the following.

There is also a direct coupling tensor $\mathsf{D}_{AB}$ for a pair of nuclei which is independent of the electronic structure of the molecule under consideration. Its elements depend on the internuclear distances and the orientation of the molecule with respect to the chosen coordinate system and can thus be employed for structural information [15]. It also becomes important in solid state or liquid crystal NMR experiments, or in cases when the molecules are (partially) aligned by a strong external field. However, for rapidly and freely rotating molecules (gas phase or solution) $\mathsf{D}_{AB}$ does not contribute to the observed

coupling and shielding constants and shall therefore not be considered further. The indirect coupling constant as well as the nuclear shielding arise from the presence of the electrons in the molecule and thus carry a wealth of chemical information which is now routinely being extracted from convenient measurements in solution.

### 2.2 NMR parameters defined as second–order energy perturbations

In this and the following subsections we are assuming either the knowledge of a hypothetical exact wavefunction or electron density, or when referring to existing methodology, the knowledge of an approximate wavefunction or electron density that has been determined such as to minimize the energy (variational approach). This is not a necessary condition in order to calculate molecular properties in general and NMR parameters in particular, however it facilitates qualitative discussions and interpretations based on wavefunction or electron density perturbations. For a more general account of calculations of energy derivatives the reader is referred to Ref. 17.

In first–principles quantum theories of molecules, a system is characterized by its potential (nuclear coordinates and charges), its number of electrons and its kinematics (the form of the operators for the kinetic energy and the electronic repulsion, for instance nonrelativistic vs. relativistic expressions). Therefore, a transition metal complex is formally treated the same way as other molecules. The shielding and indirect spin–spin coupling tensors are thereby obtained as double first–order perturbations of the total energy $E$ of the molecule. In variational wavefunction based methods,

$$E = \langle \Psi | \hat{H} | \Psi \rangle \quad , \tag{4}$$

with $\Psi$ being the normalized wavefunction. In Kohn–Sham density functional theory (DFT),

$$E = E[\rho] \quad ; \quad \rho = \sum_{i}^{\mathrm{occ}} \varphi_i^* \varphi_i \quad , \tag{5}$$

with $\rho$ being the electron density and the $\varphi_i$ the occupied Kohn–Sham molecular orbitals (MOs). $E[\rho]$ indicates that $E$ is a functional of the density. It should be noted that in Kohn–Sham DFT the kinetic energy is not calculated from the density. For NMR calculations, the two perturbation parameters are $\boldsymbol{\mu}_A$, and $\boldsymbol{\mu}_B$ or $\mathbf{B}^{\mathrm{ext}}$, respectively, i.e.

$$\boldsymbol{\sigma}_A = \left. \frac{\partial^2 E}{\partial \boldsymbol{\mu}_A \partial \mathbf{B}^{\mathrm{ext}}} \right|_{\boldsymbol{\mu}_A = 0, \mathbf{B}^{\mathrm{ext}} = 0} \tag{6a}$$

$$\mathsf{K}_{AB} = \left. \frac{\partial^2 E}{\partial \boldsymbol{\mu}_A \partial \boldsymbol{\mu}_B} \right|_{\boldsymbol{\mu}_A = 0, \boldsymbol{\mu}_B = 0} \quad . \tag{6b}$$

In (6a) the energy is supposed not to contain the classical nuclear Zeeman term $-\boldsymbol{\mu}_A \mathbf{B}^{\mathrm{ext}}$ which accounts for the "1" in Eq. (1a). Note the formal agreement of Eqs. (6a,6b) with the respective derivatives of Eqs. (1a,1b). These two equations are obtained first by deriving an expression of the molecular energy $E$ which includes all terms in the molecular quantum Hamiltonian $\hat{H}$ that are related to the nuclear magnetic moments and the external field $\mathbf{B}^{\mathrm{ext}}$, and second by considering their interaction with the magnetic moments arising from the electronic spins and their motion through space. Accordingly,

$\Psi$ or $\rho$ must be understood as being dependent on $\boldsymbol{\mu}_A$, $\boldsymbol{\mu}_B$ and $\mathbf{B}^{\text{ext}}$. Integration over all electronic degrees of freedom yields expressions of the same formal structure as (1a,1b). Thus the combined terms of explicit expressions for Eq. (4) or (5) that are bilinear in $\boldsymbol{\mu}_A$ and $\boldsymbol{\mu}_B$ correspond to Eq. (1b) and yield $\mathsf{K}_{AB}$ upon differentiation, whereas the terms that are bilinear in $\boldsymbol{\mu}_A$ and $\mathbf{B}^{\text{ext}}$ correspond to (1a) and yield $\boldsymbol{\sigma}_A$.

Taking the derivatives of $E$ with respect to $\boldsymbol{\mu}_A$ and $\boldsymbol{\mu}_B$ or $\mathbf{B}^{\text{ext}}$ involves first to take the derivatives of the operators that constitute the Hamiltonian $\hat{H}$ or the Kohn–Sham density functional and that are dependent on $\boldsymbol{\mu}_A$ and/or $\boldsymbol{\mu}_B$ and/or $\mathbf{B}^{\text{ext}}$. They can be derived once a particular (relativistic or nonrelativistic) Hamiltonian or density functional has been adopted. Second, the presence of the magnetic perturbations in the Hamiltonian causes (small) changes in the electronic structure (i.e. $\Psi$ or $\rho$) that need to be taken into account to first order in order to calculate the second–order perturbations of the energy. Thus, derivatives of the wavefunction $\Psi$ or the electron density $\rho$ , with respect to at least one of the perturbations, are additionally required. Here, the particular form of energy expression within different ab–initio methods, but also DFT (e.g. density vs. current–density functionals), is crucial for obtaining the correct equations for these perturbations.

The notation in Eqs. (6a,6b) corresponds to the usual notation of perturbation theory [18] in which it is understood that the derivatives of the Hamiltonian as well as all variational and nonvariational parameters (i.e. including the dependence of the wavefunction on the perturbations) are taken. Some authors prefer to write Eqs. (6a,6b) as total derivatives of $E$ in order to indicate that all dependencies of $E$ on the perturbation parameters must be considered [19, 20]. Ultimately one needs to consider an explicit energy expression in which no hidden dependencies on any of the perturbations are left. This also includes a possible dependence of the basis set on the perturbation.

### 2.3 The gauge problem

Any DFT computations of NMR properties of molecules with present–day program codes requires either the use of a finite basis set (or a finite number of points on a grid, or both) to represent the molecular orbitals. Obviously, no complete (infinite size) basis can be employed, which has some important consequences for basis set calculations of $\boldsymbol{\sigma}_A$, generally known as the "gauge dependence" or "gauge origin" problem. This applies to other molecular properties related to a $\mathbf{B}^{\text{ext}}$ perturbation also. It is introduced via the magnetic vector potential $\mathbf{A}^{\text{ext}}$ related to $\mathbf{B}^{\text{ext}} = \boldsymbol{\nabla} \times \mathbf{A}^{\text{ext}}$ which directly enters the magnetic terms in the Hamiltonian. Here we do not want to elaborate on the origin of the gauge problem but refer to some recent overview articles for details [19, 21]. See also McWeeny's textbook [22]. For the purpose of this article it is sufficient to mention that a "gauge dependence" of $\boldsymbol{\sigma}_A$ arises from using an incomplete basis set. It makes the shielding tensor more or less strongly dependent on the chosen origin of the coordinate system for the computation. This renders a comparison of nuclear shieldings within a molecule, or between nuclei of different molecules that are not put at the same coordinates, questionable. Generally, the better the basis set is, the less pronounced is the origin dependence of $\boldsymbol{\sigma}_A$ due to the gauge problem. However, the convergence of the results with respect to the basis size is slow and also small differences of chemical shifts are meaningful, important and experimentally detectable.

Additional terms in explicit expressions for the shielding tensor, either in the atomic basis set or at some intermediate level, are deliberately introduced in order to remove or reduce the origin dependence of $\boldsymbol{\sigma}_A$. The larger the basis set becomes, the less important become these contributions. Curing

the gauge problem in the formalism has the additional advantage that this effectively leads to well converged results for shielding tensors even with moderately sized basis sets [17], though a program implementation is somewhat more involved. There are a number of different methodologies available that are concerned with the origin dependence, among them the use of "gauge including atomic orbitals" (GIAO), of an "individual gauge of localized orbitals" (IGLO), a "localized orbital / local origin" (LORG), or applying a "continuous set of gauge transformations" (CSGT). See Sec. 3 for references. It is now widely recognized that nuclear shieldings computations should in some way include gauge correction terms, with the GIAO method being among the most effective and widespread. In this method, the atomic basis functions are chosen to depend on $\mathbf{B}^{\mathrm{ext}}$ in such a way that $\boldsymbol{\sigma}_A$ becomes origin–independent even when using a minimal basis. [1] Other methods solve the gauge problem in a different way, but they all have in common that they lead to additional contributions in $\boldsymbol{\sigma}_A$ which depend on the coordinates of the nucleus and remove or reduce the origin dependency. Such approaches are commonly referred to as "distributed gauge origin" (DGO) methods, as compared to adopting a "common gauge origin" (CGO).

### 2.4 The 2n+1– and the interchange–theorem

When calculating the second derivatives of $E$ in a variational formalism, use can be made of the so–called $(2n+1)$ theorem and the interchange theorem [18]. The $(2n+1)$ theorem states that the availability of the $n$-th order perturbation of the wavefunction or electron density allows the calculation of the perturbed energy up to order $2n+1$. The interchange theorem states that the order in which the derivatives are taken in Eqs. (6a,6b) is arbitrary. This means that only the derivative of $\Psi$ or $\rho$ with respect to $\boldsymbol{\mu}_A$ *or* $\mathbf{B}^{\mathrm{ext}}$ is needed, not both, in order to calculate the nuclear shielding. The respective perturbed $\Psi$ or $\rho$ is in turn calculated from expanding their defining equation(s) (Kohn–Sham equations, Hartree–Fock equations, ..., Schrödinger equation) in a power series with respect to the perturbation parameters and collecting terms linear in the chosen perturbation. The solution of this / these equation(s) represents the main computational task in the determination of $\boldsymbol{\sigma}_A$ or $\mathsf{K}_{AB}$ and is often similarly expensive as finding the unperturbed (zeroth–order) wavefunction or electron density. The latter must be known prior to carrying out a NMR calculation. For reasons of computational efficiency, in nuclear shielding computations the perturbation equation(s) is / are solved with $\mathbf{B}^{\mathrm{ext}}$ as the perturbation, since the shielding tensors for all the nuclei in the molecule can subsequently be determined without too much additional computational cost. In calculations of $\mathsf{K}_{AB}$, a perturbed $\Psi$ or $\rho$ must be available for one of the nuclei for each pair $A$, $B$ of interest. The result is independent of which nucleus is the "perturbing", i.e. for which nucleus the perturbed $\Psi$ or $\rho$ is calculated.

### 2.5 Perturbation operators

Let $\hat{H}^{(\boldsymbol{\mu}_A)}$ collectively denote the all "magnetic" operators that contribute to the first derivative of $\hat{H}$ with respect to $\boldsymbol{\mu}_A$ at $\boldsymbol{\mu}_A = \boldsymbol{\mu}_B = \mathbf{B}^{\mathrm{ext}} = 0$. Accordingly, $\hat{H}^{(\boldsymbol{\mu}_B)}$ and $\hat{H}^{(\mathbf{B}^{\mathrm{ext}})}$ are the derivatives with respect to $\boldsymbol{\mu}_B$ and $\mathbf{B}^{\mathrm{ext}}$, respectively, and $\hat{H}^{(\boldsymbol{\mu}_A,\boldsymbol{\mu}_B)}$ etc. denote the mixed second derivatives. Further, $\hat{h}^{(\boldsymbol{\mu}_A)}$ shall denote a respective one–electron operator, i.e. $\hat{H}^{(\boldsymbol{\mu}_A)} = \sum_{i=1}^{N} \hat{h}^{(\boldsymbol{\mu}_A)}(i)$ + two–electron terms, if applicable. $N$ is the number of electrons in the system. In Tab. 1, a number of *nonrelativistic*

[1] It is a different question whether results obtained with small basis sets, even if origin independent, are meaningful at all

Table 1: Nonrelativistic one–electron "magnetic" terms in the Hamiltonian. Their derivatives with respect to $\boldsymbol{\mu}_A$ and/or $\mathbf{B}^{\text{ext}}$ or $\boldsymbol{\mu}_B$ enter the expressions for the nuclear shielding and spin–spin coupling tensors via the perturbation operators $\hat{h}^{(\boldsymbol{\mu}_A)}$, $\hat{h}^{(\boldsymbol{\mu}_B)}$, $\hat{h}^{(\mathbf{B}^{\text{ext}})}$, $\hat{h}^{(\boldsymbol{\mu}_A,\mathbf{B}^{\text{ext}})}$ and $\hat{h}^{(\boldsymbol{\mu}_A,\boldsymbol{\mu}_B)}$. $\hat{\mathbf{S}}$ is the spin–operator for an electron, $\mathbf{r}_A$ a distance vector with respect to nucleus $A$ etc.

| Operator | Name | Contributes to |
|---|---|---|
| $\hat{h}^{OZ} = -\frac{i}{2}\mathbf{B}^{\text{ext}} \cdot (\mathbf{r} \times \boldsymbol{\nabla})$ | Orbital Zeeman | $\hat{h}^{(\mathbf{B}^{\text{ext}})}$ |
| $\hat{h}^{SZ} = \mathbf{B}^{\text{ext}} \cdot \hat{\mathbf{S}}$ | Spin-Zeeman [a] | $\hat{h}^{(\mathbf{B}^{\text{ext}})}$ |
| $\hat{h}^{OP} = -\frac{i}{c^2}\sum_A \boldsymbol{\mu}_A\big(\frac{\mathbf{r}_A}{r_A^3} \times \boldsymbol{\nabla}\big)$ | Paramagnetic Orbital [b] | $\hat{h}^{(\boldsymbol{\mu}_A)}, \hat{h}^{(\boldsymbol{\mu}_B)}$ |
| $\hat{h}^{FC} + \hat{h}^{SD} = \frac{1}{c^2}\sum_A \hat{\mathbf{S}}\big[\boldsymbol{\mu}_A(\boldsymbol{\nabla} \cdot \frac{\mathbf{r}_A}{r_A^3}) - (\boldsymbol{\mu}_A \cdot \boldsymbol{\nabla})\frac{\mathbf{r}_A}{r_A^3}\big]$ | | $\hat{h}^{(\boldsymbol{\mu}_A)}, \hat{h}^{(\boldsymbol{\mu}_B)}$ |
| $\hat{h}^{FC} = \frac{8\pi}{3c^2}\sum_A \delta(\mathbf{r}_A)\boldsymbol{\mu}_A \cdot \hat{\mathbf{S}}$ | Fermi Contact [a] | $\hat{h}^{(\boldsymbol{\mu}_A)}, \hat{h}^{(\boldsymbol{\mu}_B)}$ |
| $\hat{h}^{SD} = \frac{1}{c^2}\sum_A r_A^{-5}\big[3(\hat{\mathbf{S}} \cdot \mathbf{r}_A)(\boldsymbol{\mu}_A \cdot \mathbf{r}_A) - r_A^2\boldsymbol{\mu}_A \cdot \hat{\mathbf{S}}\big]$ | Spin–Dipole [a] | $\hat{h}^{(\boldsymbol{\mu}_A)}, \hat{h}^{(\boldsymbol{\mu}_B)}$ |
| $\hat{h}^{DS} = \frac{1}{2c^2}\sum_A \big[(\boldsymbol{\mu}_A \cdot \mathbf{B}^{\text{ext}})(\frac{\mathbf{r}_A}{r_A^3} \cdot \mathbf{r}) - (\boldsymbol{\mu}_A \cdot \mathbf{r})(\mathbf{B}^{\text{ext}} \cdot \frac{\mathbf{r}_A}{r_A^3})\big]$ | Diamagnetic Shielding | $\hat{h}^{(\boldsymbol{\mu}_A,\mathbf{B}^{\text{ext}})}$ |
| $\hat{h}^{OD} = \frac{1}{2c^4}\sum_{B\neq A} r_A^{-3} r_B^{-3}\big[(\boldsymbol{\mu}_A \cdot \boldsymbol{\mu}_B)(\mathbf{r}_A \cdot \mathbf{r}_B) - (\boldsymbol{\mu}_A \cdot \mathbf{r}_B)(\boldsymbol{\mu}_B \cdot \mathbf{r}_A)\big]$ | Diamagnetic Orbital [c] | $\hat{h}^{(\boldsymbol{\mu}_A,\boldsymbol{\mu}_B)}$ |

[a] No contribution to $\boldsymbol{\sigma}_A$ in nonrelativistic or scalar relativistic calculations excluding spin–orbit coupling

[b] Also called "Paramagnetic Spin–Orbit" (PSO), referring to nuclear spins and electronic orbits

[c] Also called "Diamagnetic Spin–Orbit" (DSO), see also [b]

one–electron terms in the molecular Hamiltonian are listed that yield these perturbation operators upon differentiation, which in turn enter the expressions for $\boldsymbol{\sigma}_A$ and $\mathsf{K}_{AB}$. Relativistic operators are discussed in Refs. [6–8]. There, the reader can also find literature references where the perturbation operators for specific relativistic methodologies are explicitly listed.

### 2.6 The sum–over–states (SOS) formula

Let us for reasons of simplicity not consider any particular expression for the energy $E$ at this point. As already mentioned, for the computation of the nuclear shielding $\boldsymbol{\sigma}_A$, one needs $\Psi^{(\mathbf{B}^{\text{ext}})}$, the first–order derivative of the wavefunction with respect to the external field at $\boldsymbol{\mu}_A = 0, \mathbf{B}^{\text{ext}} = 0$. For the computation of the coupling constant, knowledge of $\Psi^{(\boldsymbol{\mu}_A)}$ is required. Let $\Psi_0$ be the unperturbed wavefunction of the ground state of the molecule, or the reference state, for which the NMR property is to be calculated. The shielding tensor is then given by differentiating Eq. (4) in the sense of (6a), which directly yields

$$\begin{aligned}\boldsymbol{\sigma}_A &= \langle\Psi_0|\hat{H}^{(\boldsymbol{\mu}_A,\mathbf{B}^{\text{ext}})}|\Psi_0\rangle + \langle\Psi^{(\mathbf{B}^{\text{ext}})}|\hat{H}^{(\boldsymbol{\mu}_A)}|\Psi_0\rangle + \langle\Psi_0|\hat{H}^{(\boldsymbol{\mu}_A)}|\Psi^{(\mathbf{B}^{\text{ext}})}\rangle \\ &= \langle\Psi_0|\hat{H}^{(\boldsymbol{\mu}_A,\mathbf{B}^{\text{ext}})}|\Psi_0\rangle + 2\,\text{Re}\langle\Psi^{(\mathbf{B}^{\text{ext}})}|\hat{H}^{(\boldsymbol{\mu}_A)}|\Psi_0\rangle \quad . \end{aligned} \tag{7a}$$

Here, the terminology of Sec. 2.5 has been adopted. The first term in (7a) is called the diamagnetic shielding, the second term is called the paramagnetic shielding. This subdivision depends on the choice of gauge of the magnetic vector potential (here: Coulomb gauge) and refers to the nonrelativistic theory of nuclear shielding. Additional contributions might be contained in the expression if $\hat{H}$ and $E$ refer to a relativistic formalism, in particular those due to the electronic spin–orbit coupling. The latter belong to the "paramagnetic" type. In a four–component formalism there is no explicit diamagnetic term in the respective equation.

The reduced indirect spin–spin coupling tensor is given by

$$\begin{aligned}\mathsf{K}_{AB} &= \langle\Psi_0|\hat{H}^{(\boldsymbol{\mu}_A,\boldsymbol{\mu}_B)}|\Psi_0\rangle + \langle\Psi^{(\boldsymbol{\mu}_A)}|\hat{H}^{(\boldsymbol{\mu}_B)}|\Psi^{(0)}\rangle + \langle\Psi_0|\hat{H}^{(\boldsymbol{\mu}_B)}|\Psi^{(\boldsymbol{\mu}_A)}\rangle \\ &= \langle\Psi_0|\hat{H}^{(\boldsymbol{\mu}_A,\boldsymbol{\mu}_B)}|\Psi_0\rangle + 2\,\text{Re}\langle\Psi^{(\boldsymbol{\mu}_A)}|\hat{H}^{(\boldsymbol{\mu}_B)}|\Psi_0\rangle \quad . \end{aligned} \tag{7b}$$

Again, the first term in (7b) is commonly referred to as the diamagnetic coupling contribution, diamagnetic orbital term (OD), or diamagnetic (nuclear) spin – (electronic) orbit term (DSO). The second term contains, in a nonrelativistic theory, the Fermi–contact (FC), the spin–dipole (SD) and the FC–SD cross term, as well as the paramagnetic orbital term (OP or PSO). In a relativistic theory, spin–orbit contributions are further included (e.g. the FC–OP cross term). In deriving both expressions, (7a) and (7b), use has been made of the Hellmann-Feynman theorem [23] which allows to avoid the computation of a second derivative of the wavefunction (as mentioned before in the context of the $(2n + 1)$ theorem). Note the equal formal structure of the two equations, which is in fact the same for all time–independent second–order perturbations of the energy [4].

The operators as well as the unperturbed wavefunction are supposed to be known, thus the only unknown quantities in (7a) and (7b) are $\Psi^{(\mathbf{B}^{\text{ext}})}$ and $\Psi^{(\boldsymbol{\mu}_A)}$, respectively. In the *sum–over–states* (SOS) approach, all the unperturbed excited states wavefunctions $\Psi_j$ are now used as a convenient complete orthonormal basis set in which to expand the perturbed wavefunctions of the ground state. By considering only first–order terms in the (relativistic or nonrelativistic) wave equation, the following expression for $\Psi^{(\mathbf{B}^{\text{ext}})}$ is readily derived:

$$\Psi^{(\mathbf{B}^{\text{ext}})} = \sum_{j\neq 0} \frac{\langle\Psi_j|\hat{H}^{(\mathbf{B}^{\text{ext}})}|\Psi_0\rangle}{E_0 - E_j}\Psi_j \tag{8}$$

The expression for $\Psi^{(\boldsymbol{\mu}_A)}$ is obtained by changing $\hat{H}^{(\mathbf{B}^{\text{ext}})}$ to $\hat{H}^{(\boldsymbol{\mu}_A)}$. When these results are substituted in Eqs. (7a) and (7b), the following (in principle exact) SOS expressions for the NMR observables are obtained:

$$\boldsymbol{\sigma}_A = \langle\Psi_0|\hat{H}^{(\boldsymbol{\mu}_A,\mathbf{B}^{\text{ext}})}|\Psi_0\rangle + 2\sum_{j\neq 0}\text{Re}\,\frac{\langle\Psi_0|\hat{H}^{(\mathbf{B}^{\text{ext}})}|\Psi_j\rangle\langle\Psi_j|\hat{H}^{(\boldsymbol{\mu}_B)}|\Psi_0\rangle}{E_0 - E_j} \tag{9a}$$

$$\mathsf{K}_{AB} = \langle\Psi_0|\hat{H}^{(\boldsymbol{\mu}_A,\boldsymbol{\mu}_B)}|\Psi_0\rangle + 2\sum_{j\neq 0}\text{Re}\,\frac{\langle\Psi_0|\hat{H}^{(\boldsymbol{\mu}_A)}|\Psi_j\rangle\langle\Psi_j|\hat{H}^{(\boldsymbol{\mu}_B)}|\Psi_0\rangle}{E_0 - E_j} \tag{9b}$$

Of course in practice not all, usually not even one, of the excited states wavefunctions are known. Therefore, Eqs. (9a) and (9b) as they stand do not have much practical importance. However they greatly facilitate interpretations. For instance, systems with low lying exited states are likely to have larger values for their NMR observables (and other second–order properties). Trends among related compounds for magnetic properties can often be rationalized by trends observed for the excitation energies. For instance, $^{95}$Mo chemical shifts in a number of complexes were in Ref. 24 shown to correlate very well with the energy of the lowest–lying magnetically allowed excitation. By knowing the form of the perturbation operators it is also often possible to make qualitative predictions on the size of the matrix elements in the numerator of the SOS expression, which might yield useful interpretations. Based on the nonrelativistic formalism it can easily be deduced from symmetry arguments that in atoms there is no paramagnetic contribution to the shielding tensor, and that in linear molecules the paramagnetic principal components of the $\boldsymbol{\sigma}_A$ and $\mathsf{K}_{AB}$ tensors are zero along the molecular axis.

### 2.7 Density functional theory (DFT)

In Kohn–Sham–DFT–based approaches, expressions that are of similar structure as (9a) and (9b) are obtained, but in form of contributions from all occupied Kohn–Sham MOs $\varphi_i$. The excited states wavefunctions are at the same time *formally* replaced by the unoccupied MOs, and the many–electron perturbation operators $\hat{H}^{(\boldsymbol{\mu}_A)}$ etc. by their one–electron counterparts $\hat{h}^{(\boldsymbol{\mu}_A)}$ etc. Orbital energies $\varepsilon_i$ and $\varepsilon_a$ formally substitute the total energies of the states (see below). Thus, similar interpretations of NMR parameters can be worked out in which the HOMO–LUMO gap (HLG) plays a highly important role. It must be emphasized, though, that there is no one–to–one correspondence between the excited states of the SOS equations and the unoccupied orbitals which enter the DFT expressions, nor between excitation energies and orbital energy differences. I.e. there are no one–determinantal "wavefunctions" in Kohn–Sham–DFT perturbation theory which approximate the reference and excited states.

In formal analogy to the perturbed $\Psi^{(\boldsymbol{\mu}_A)}$ etc., in Kohn–Sham DFT there are the perturbations $\varphi_i^{(\boldsymbol{\mu}_A)}$ etc. of the occupied MOs that are in turn represented in the complete orthonormal basis of all unperturbed MOs. The occupied orbitals enter the expressions for the effective Hartree + exchange–correlation (HXC) potential $V_{HXC}$ of the molecule which originates from the electron–electron Coulomb interaction and the Pauli principle. Because of the orbitals being perturbed, in addition to the "external" perturbation (magnetic field or nuclear spin) there is also a "coupled" perturbation contribution $V_{HXC}^{(\mathbf{B}^{\text{ext}})}$ or $V_{HXC}^{(\boldsymbol{\mu}_A)}$ (similar to coupled Hartree-Fock theory). Considering such terms, the DFT equa-

tions for $\boldsymbol{\sigma}_A$ and $\mathsf{K}_{AB}$ read

$$\boldsymbol{\sigma}_A = \sum_i^{\text{occ}} \langle\varphi_i|\hat{h}^{(\boldsymbol{\mu}_A,\mathbf{B}^{\text{ext}})}|\varphi_i\rangle + 2\sum_i^{\text{occ}}\sum_a^{\text{unocc}} \text{Re}\,\frac{\langle\varphi_i|\hat{h}^{(\mathbf{B}^{\text{ext}})} + V_{HXC}^{(\mathbf{B}^{\text{ext}})}|\varphi_a\rangle\langle\varphi_a|\hat{h}^{(\boldsymbol{\mu}_B)}|\varphi_i\rangle}{\varepsilon_i - \varepsilon_a} \tag{10a}$$

$$\mathsf{K}_{AB} = \sum_i^{\text{occ}} \langle\varphi_i|\hat{h}^{(\boldsymbol{\mu}_A,\boldsymbol{\mu}_B)}|\varphi_i\rangle + 2\sum_i^{\text{occ}}\sum_a^{\text{unocc}} \text{Re}\,\frac{\langle\varphi_i|\hat{h}^{(\boldsymbol{\mu}_A)} + V_{HXC}^{(\boldsymbol{\mu}_A)}|\varphi_a\rangle\langle\varphi_a|\hat{h}^{(\boldsymbol{\mu}_B)}|\varphi_i\rangle}{\varepsilon_i - \varepsilon_a} \tag{10b}$$

and are in principle exact, though as usual in DFT the XC contribution is only known to some approximation. An exact (complete basis) representation of the orbitals is assumed, therefore (10a,10b) do not include any of the aforementioned "gauge terms". With functionals that do not depend on the current–density the contribution $V_{HXC}^{(\mathbf{B}^{\text{ext}})}$ is zero. We will in the following refer to such cases as "uncoupled" DFT perturbation methods. It should be noted that this notion refers to non–hybrid functionals that depend on the density, its gradients and higher derivatives, or the kinetic energy density, but not to hybrid functionals that inclde Hartree–Fock exchange. In the latter case a coupled perturbed $V_{HXC}^{(\mathbf{B}^{\text{ext}})}$ corresponding to the fraction of Hartree–Fock exchange in the hybrid functional is usually included in the NMR computations. Regarding fully coupled perturbed current–density functional methods applied to NMR calculations not much data are available in the literature. It appears that the contributions from the current–density dependent part of the functional are negligible [25], which somewhat justifies the common uncoupled approach. On the other hand, so far only comparatively simple current–density functionals have been applied in such investigations. It is presently not clear whether the current–density dependent coupled terms will gain importance when more sophisticated functionals are applied or whether they can become large, for instance, for other compounds that that were tested so far (e.g. they might be important for chemical shifts of transition metals). So–called SOS–DFT has been devised [26,27] in which the orbital–energy denominators of the DFT expression are replaced by approximate excitation energies, in order to cure some of the deficiencies of the various available non–hybrid XC potentials. This approach has found some justification by producing more accurate results in a number of applications, but has also been criticized for its semi–empirical nature. Recently, similar expressions have been obtained not by resorting to the SOS argument but from an argument based on time–dependent DFT methods, in an attempt to derive equivalent TDDFT analogs for the SOS expression for electric and magnetic perturbations [28,29]. Attempts have further been made to obtain improved NMR parameters by self interaction corrected (SIC) DFT [30,31] and other "non–standard" Kohn–Sham potentials (e.g. in Ref. 32). There are currently not enough data available in order to judge their performance for transition metal complexes.

As already mentioned, the MOs in Eqs. (10a,10b) are assumed to be exact, i.e. represented at the complete basis set limit. In practice, the Kohn–Sham equations are converted into the respective SCF matrix equations in the basis, and the perturbation treatment is carried out from there. Any dependence of the basis set (GIAOs) on the perturbation ($\mathbf{B}^{\text{ext}}$ in the case of shielding tensors) is in this way naturally covered.

### 2.8 Singlet and triplet perturbations, spin–orbit coupling

Some of the perturbation operators in Tab. 1 do not depend on the electron spin. As a consequence, integration over spin can be carried out in Eqs. (9a) and (9b) for all terms that contain only these

spin–free operators. They yield zero in a nonrelativistic or scalar relativistic framework (i.e. without spin–orbit coupling) unless $\Psi_j$ is a singlet excited state ($\Psi_0$ is supposed to be a singlet closed-shell ground state). Similar arguments apply to the contributions from spin–up and spin–down MOs in Eqs. (10a) and (10b). Such perturbations are often referred to as "singlet perturbations". The spin–dependent perturbations are referred to as "triplet perturbations" and only yield nonzero contributions from excited triplet states in the perturbed wavefunction, compare Eq. (8). This means that such a perturbation also causes a spin–polarization of the closed–shell ground state. The Fermi–contact operator in Tab. 1 is an example. Without spin–orbit coupling, for a closed shell molecule all cross terms where in the SOS equation or in (10a) and (10b) one of the perturbation operators is a singlet, the other one a triplet perturbation exactly cancel due to contributions of equal magnitude but opposite sign from the spin–up and spin–down orbitals, respectively. Therefore, the FC and SD operators do not contribute to the shielding tensor at this level of theory.

In case there is spin–orbit (SO) coupling present, the orbitals or the density of the system can in general not anymore be divided into purely spin–up or –down contributions but there are contributions from both. The action of a singlet–perturbation, for example $\hat{H}^{(\mathbf{B}^{\mathrm{ext}})}$, then leads to different results for the spin–up and the spin–down portion of the orbitals. This in turn causes a spin–density in the molecule to be induced by a singlet perturbation. For instance, when spin–orbit coupling is considered the external field (OZ operator) yields cross terms with the FC and SD terms, which represents the most important spin–orbit effect on the nuclear shielding [33–35]. Likewise, for the spin–spin coupling tensor there occur cross terms between FC or SD and the singlet OP term.

### 2.9 Relativistic methods

So far no specification has been made whether the energy expression on which the NMR calculation is based is relativistic or not. It is long known that electrons "move very fast" and, in molecules with heavy nuclei, reach a substantial portion of the speed of light. Thus, the effects of Einstein's special relativity must be considered in their theoretical description. The reader is referred to the literature for accounts of relativistic methodology for molecules [36–40] and the computation of molecular properties within such formalisms [4]. For review articles that are specifically devoted to relativistic NMR computations see Refs. 6–8. It is important to know that relativistic effects are stronger for systems with heavy nuclei (the leading order effects increase $\sim Z^2$). It depends on the accuracy of the calculation — and which quantity is calculated — whether a relativistic calculation must be carried out or not. For the 5d transition metals, relativistic corrections should generally be considered, independent of the goal of the calculation (provided the goal is not to produce qualitatively wrong answers).

For the present discussion, it is of importance that a relativistic NMR computation is carried out if $E$ in Eq. 4 is defined and calculated within a relativistic framework, otherwise it is nonrelativistic. Another approach is to treat relativity as an additional perturbation and to evaluate relativistic corrections to $\boldsymbol{\sigma}_A$ and $\mathsf{K}_{AB}$ individually in form of derivatives of (6a) and (6b) with respect to a suitably chosen relativistic perturbation parameter (usually $c^{-2}$). I.e. first a nonrelativistic NMR observable is calculated and then correction terms are obtained in the form of

$$\Delta^{\mathrm{rel}}\boldsymbol{\sigma}_A = c^{-2} \cdot \left.\frac{\partial^3 E}{\partial \mathbf{B}^{\mathrm{ext}} \partial \boldsymbol{\mu}_A \partial c^{-2}}\right|_{c\to\infty, \boldsymbol{\mu}_A=0, \mathbf{B}^{\mathrm{ext}}=0} + \mathcal{O}(c^{-4}) \tag{11}$$

and similarly for $\mathsf{K}_{AB}$. In the variational relativistic approaches, the second derivatives (6a,6b) of $E$ yield unseparated the nonrelativistic quantities plus all relativistic corrections that the scheme covers. Perturbational approaches can be advantageous for interpretational purposes (clear separation of leading ($c^{-2}$) and higher order ($c^{-4}, c^{-6} \ldots$) relativistic corrections) but it should be kept in mind that for the heaviest NMR nuclei the relativistic effects on $\boldsymbol{\sigma}$ can be huge and will not be fully covered by the terms linear in $c^{-2}$. This gives variational relativistic methods an advantage of relative conceptual simplicity over higher order relativistic perturbational approaches when computing $\boldsymbol{\sigma}_A$ or $\mathsf{K}_{AB}$ for a heavy nucleus or its neighbor atoms. If desired, a nonrelativistic calculation can always be carried out in addition in order to estimate the magnitude of the relativistic contributions.

The computation of NMR observables within a relativistic formalism has some important consequences. The most obvious is that the Hamiltonian of the system — and thus the perturbation operators — are different in a variational relativistic scheme (i.e. if relativity is not treated as a perturbation. Otherwise, the nonrelativistic operators of Tab. 1 occur in the leading–order terms). There are a number of different methodologies available for carrying out relativistic computations in a variationally stable manner. Each of them requires the implementation of a specific set of perturbation operators for the purpose of NMR calculations. It is very important to keep the method internally consistent in order to avoid singularities, variational collapse, and meaningless results. For instance, for point nuclei the FC operator yields arbitrarily large matrix elements in conjunction with relativistic MOs, whereas its relativistic analogs stay finite [8].

To the author's knowledge, four–component relativistic computations have so far not been carried out for NMR parameters of transition metal complexes, which is likely due to the formidable computational effort since respective program codes exist. Two–component methods can be more efficient and have been applied to a large range of transition metal complexes. In this paper, two–component methods are classified as to include the important effects of spin–orbit coupling, some of which will be discussed in Sec. 4. If spin–orbit coupling is neglected in a two–component Hamiltonian, the approach turns into a one–component, so–called scalar relativistic one. Presently, for transition metal systems the most frequently applied two–component relativistic DFT NMR method is based on the zeroth–order regular approximation (ZORA) [41–46]. Nuclear shieldings have further successfully been computed based on the second–order Douglas-Kroll-Hess (DKH2) transformed Hamiltonian [40, 47–50]. A variationally not stable approach using the two–component Pauli–Hamiltonian in conjunction with frozen cores has for some years been utilized [2, 51–53], but is now depreciated in favor of variationally stable methods. In the following, this method will be designated by vPSC if only scalar relativistic effects are considered, otherwise by vPSCSO. Perturbational results based on Eq. (11) will be mentioned in Sec. 4 as well. They have so far employed the Pauli operator and will be designated by pPSC or pPSCSO, respectively.

Besides these direct relativistic methods, the relativistic effects on a heavy atom's valence shell can also be incorporated in an otherwise nonrelativistic computation by employing effective core potentials (ECPs) for the heavy atom. As long as the core shell of the heavy elements is not of particular interest (i.e. for structure, energetics and most properties except electric and magnetic properties related to the heavy nucleus or the core shells of the heavy atom) such computations are very efficient and accurate [54]. For example, ligand chemical shift or coupling constants between the ligands of a heavy metal can be calculated this way without the need for a specific relativistic program development. However, two–component ECPs which allow to recover the effects of spin–orbit coupling in the heavy atom's valence shell are not in such widespread use.

## 3 Program developments for NMR computations

### 3.1 The pre–DFT era

Already by the late 1970s a large number of review articles on NMR calculations were available. They have recently been collected in a meta–review [55]. Most of the theoretical calculations up to that time were concerned with small organic and inorganic main group systems, while transition metal systems were generally treated with the help of more or less sophisticated methodologies based on ligand field theory [56]. In 1978 De Brouckere published a 100 pages overview with 289 references that was devoted to the LCAO-SCF-MO computation of properties of transition metal complexes [57]. This included NMR parameters. Both in the case of nuclear shieldings and spin–spin coupling constants De Brouckere found that such calculations had never been carried out for transition metal systems.

The reader is referred to Ref. 58 for early work on NMR properties based on the Hartree–Fock approach. For instance, in this collection Nakatsuji presented the calculation of shielding constants of transition metals. It has later been concluded that the Hartree–Fock approach is in general not adequate for this purpose, though it might be reasonable in the special case of high metal oxidation states or $d^{10}$ systems [1].

### 3.2 DFT program developments for NMR parameters

During the 1980s, NMR shielding codes were developed based on the Hartree–Fock–Slater (HFS or X$\alpha$) method, which is now being classified as DFT [59–61]. Computational restrictions did not allow at that time to use adequate basis sets in order to yield accurate chemical shifts for the small, light atomic, systems that could be studied. For the same reasons, transition metal complexes were still out of reach. Further, from the results it was concluded that coupled Hartree–Fock is superior to the X$\alpha$ method [59]. $^{13}$C shielding constants were found to have inaccurate magnitudes, though the trends among various small molecules were, according to the authors, reproduced remarkably well [60]. A pioneering FPT-X$\alpha$ study of spin–spin coupling constants in 1976 (only the FC term implemented) did not yield any agreement with experimental data for $H_2$ and HF, though reasonable agreement with other theoretical data was obtained.

It is clear that these early DFT attempts were suffering from basis set limitations. At the same time, the advantages of having a post–Hartree-Fock method available that is on the one hand potentially accurate enough to treat the NMR properties of transition metal systems [3, 62], and on the other hand computationally feasible (as compared to more accurate but also more expensive ab–initio methods), could not be explored. The first modern Kohn–Sham DFT implementation for nuclear shieldings was reported in 1993 [26, 63] and employed the IGLO method in order to treat the gauge problem. The LORG approach was implemented in 1994 within the DFT framework [64]. GIAO DFT implementations were soon to follow, see Refs. 25 and 65–67. The approach of Ref. 67 was also capable of handling hybrid functionals and additionally reported results obtained with the CSGT method. It did not take long before these programs were applied to a vast number of transition metal systems. The DFT computation of spin–spin coupling constants was initially implemented in 1994 by Malkin et al. [68], followed by Dickson & Ziegler in 1996 [69]. Both used a finite–perturbation approach for the FC term. The SD term was not implemented. The first analytic (non–hybrid) DFT implementation for spin–spin coupling constants (excluding the SD term) appeared only rather recently [45] and was

also capable of accurately treating scalar relativistic effects. In fact it had been the huge, variationally unstable, FC matrix elements that did not permit a finite–perturbation treatment for the heavy atomic systems that the program was intended for. An extension of the method in order to include the SD term and spin–orbit coupling was subsequently published [46]. At the same time, two nonrelativistic analytic DFT implementations (incl. SD) were reported which could additionally treat hybrid functionals as well [70, 71]. The B3LYP hybrid functional was shown to yield very promising results for small light atomic molecules, in particular those difficult ones [30] that are not well described by non–hybrid functionals.

### 3.3 Relativistic DFT NMR methods

It has been known for a long time [33, 72] that relativistic effects can have a pronounced influence on NMR observables. Therefore, relativistic DFT methods have been developed soon after the first nonrelativistic codes were available. A significant number of DFT studies, in particular many on transition metal systems, have focused on relativistic effects on NMR parameters, their origin, and their interpretation. For a detailed account of the methodology development, early and recent applications, and ab–initio as well as semi–empirical relativistic NMR methods the reader is referred to Refs. [6–8]. The first approach within the DFT framework has been to include a scalar relativistic ECP for the metal of a complex when calculating the chemical shift for a ligand nucleus, see Kaupp et al., Refs. 73, 74. Numerous applications to transition metal complexes have been carried out using this method (which does not require a relativistic NMR code) [1], some of which will be mentioned later. Schreckenbach & Ziegler have implemented chemical shifts computations based on the scalar relativistic Pauli operator and frozen cores. This method could also be applied to metal shifts and was later extended by Wolff & Ziegler to include spin–orbit coupling [52]. The DFT computation of shielding constants based on the two–component ZORA Hamiltonian was implemented by Wolff et al. [43, 44]. The author is not aware of DFT computations of NMR observables for transition metal complexes based on the four–component Dirac or the two–component DKH2 Hamiltonians (Hartree–Fock calculations, mainly on main–group systems but also, with DKH2, on small Hg complexes, have already been reported [47, 48, 75, 76]). Consideration of the Pauli spin–orbit operator in DFT shielding computations as a perturbation, Eq. 11, has been implemented by Malkin et al. [77, 78] and been extensively used to analyze spin–orbit effects on nuclear shielding [9]. The incorporation of a spin–orbit ECP into DFT NMR shielding computation was reported by Vaara et al. in 2001 [79] A two–component ZORA DFT approach to compute nuclear spin–spin coupling constants [45, 46] has intentionally been developed with transition metal systems in mind because of the known huge influence of relativity in particular on the FC mechanism.

## 4 Applications to transition metal systems

Before entering the description of computational results that have been obtained with DFT over the last 10 years, a note on the achievable accuracy is appropriate. Except perhaps for systems that are experimentally very difficult to measure accurately, a quantitative agreement of DFT results with all significant digits that are reported from experiments is virtually never accomplished. The reason for this lies of course in the sensitivity of the NMR parameters not only to experimetal conditions but also computational approximations. For chemical shifts, the sign is usually determined correctly

(except for very small magnitudes). An agreement within 10 to 20% deviation from experiment is usually considered very good, good, satisfactory, or reasonable, depending on the publication and the quality of other available computational data. Similar considerations hold for nuclear spin–spin coupling constants, though the criteria appear to be somewhat less strict because of the difficulties to compute these quantities accurately. Better agreement must in most cases not be expected because the computations are approximate and generally do not account for many influences that affect the experimental value. On the other hand, if there is a very substantial deviation between calculated and experimental result, the present–day DFT methods can usually be trusted to an extent that such a deviation suggests that it is not the functional but the computational model (chemical environment, e.g. solvent, neglect of molecular vibrations, etc.) that is deficient. Exceptions are known, of course, for instance the case of ferrocene which will be discussed in Sec. 4.3.

Some acronyms that are frequently used in the following sections are collected in Tab. 2. Acronyms referring to individual terms in the nuclear shielding or spin–spin coupling tensor are explained in Tab. 1.

### 4.1 Computations of ligand nuclear shieldings in transition metal complexes

Already in 1995 a large number of $^{13}$C chemical shifts in transition metals were studied with the SOS–DFT method (ECPs, PW91 non–hybrid functional), yielding generally good agreement with experimental data. It is also important to note that a hybrid functional (B3LYP) did not perform better in this study than the BP non–hybrid functional. In fact for the $MO_4^{n-}$ systems B3LYP yields results that compare worse with experiment (see below).

Table 3 lists experimental and computational results that have been obtained for a number of $^{17}$O shifts in tetroxo-metallates $MO_4^{n-}$. It is certainly an intriguing demonstration of the performance of DFT for transition metal NMR calculations. Compared to the shift range that is covered by these complexes, the errors for all listed DFT methods are rather small. This is a general finding that has been reported in a larger number of studies of ligand shifts in transition metal complexes [1, 3, 80]. Relativistic effects for the heavier metals listed in Tab. 3 have been included either via ECPs or by the vPSC method and, e.g. reduce the magnitude of the oxygen shielding in $WO_4^{2-}$ by about 50%. It has been argued that SO effects are of minor importance in this case [1]. The HF method performs badly in comparison. It reproduces the trends, but they are dramatically overestimated. The MP2 results cannot be assigned any physical meaning at all. This is unfortunate since MP2 is at present the perhaps only post–Hartree–Fock ab–initio method that would be computationally feasible for NMR calculations for larger transition metal systems.

The exceptionally strongly shielded protons directly bound to a transition metal have been investigated in Ref. 81. The calculations were nonrelativistic (except for the Re system, for which the vPSC method was adopted) and employed a frozen core on the metal. Satisfactory agreement with the experimental data was obtained, as shown in Tab. 4. An analysis of the results in terms of MO contributions revealed that strong, shielding, paramagnetic currents from the adjacent metal fragments cause the large negative chemical shifts. It was found that the magnitude of the proton shielding is determined by the two paramagnetic tensor components $\sigma_{\parallel}^{p}$ and $\sigma_{\perp}^{p}$. They are denoted by the orientation of the external magnetic field with respect to the M–H bond, with $\sigma_{\perp}^{p}$ being the dominant and positive contribution. The induced current strongly reduces the magnitude of the external field component in $\perp$ direction at the position of the hydrogen (i.e. it causes an increased shielding) and is thus responsible

Table 2: Frequently used acronyms. A compilation of references for density functionals can be found, e.g., in the book by Koch and Holthausen [80]

| | |
|---|---|
| *Miscellaneous:* | |
| HF | Hartree–Fock |
| MP2 | Second–order Møller–Plesset treatment for electron correlation |
| GIAO | Gauge–including (or –independent) atomic orbitals |
| IGLO | Independent gauge for localized orbitals |
| AO, MO | Atomic orbital, molecular orbital |
| HOMO, LUMO | Highest occupied, lowest unoccupied MO |
| TMS | Tetramethyl–silane |
| *Density Functionals:* | |
| LDA | Local density approximation |
| GGA | Generalized gradient approximation |
| XC | Exchange & correlation |
| VWN | Vosko–Wilk–Nusair LDA |
| BP or BP86 | Becke 1988 Perdew 1986 non–hybrid GGA |
| LYP | Lee–Yang–Parr non–hybrid GGA |
| PBE | Perdew–Burke–Ernzerhof non–hybrid GGA |
| PW91 | Perdew–Wang 1991 non–hybrid GGA |
| B3LYP | 3–parameter hybrid GGA |
| *Relativistic approaches:* | |
| ECP | Effective core potential |
| SO | Spin–orbit, or spin–orbt coupling |
| pPSC | Perturbational treatment of scalar Pauli operator |
| vPSC | Variational (frozen core) treatment of scalar Pauli operator |
| pPSO | Perturbational treatment of Pauli–operator, SO only |
| pPSCSO | Perturbational treatment of Pauli–operator, scalar + SO |
| vPSCSO | Dito, but variational (frozen core) |
| DKH2 | Second order Douglas–Kroll-Hess transformation |
| ZORA | Zeroth–order regular approximation |

for the negative "hydridic" proton shift. The opposite effect is seen for the external field component parallel to the M–H bond. The resulting induced currents reinforce the external field at the proton. It was found that $\sigma_{\parallel}^{p}$ is negative, but smaller in magnitude than $\sigma_{\perp}^{p}$. This effect is sketched in Fig. 1.

Another set of data is compiled in Table 5. Here, the $^{13}$C chemical shifts of a series of 5d transition metal carbonyls were calculated with different relativistic DFT approaches. Both scalar relativistic effects as well as SO coupling contribute to the trend along the series. Again, good agreement with the experimental data is obtained with non–hybrid functionals. It has been shown by Wolff & Ziegler [52] that the observed trend partially results from increasingly large shielding SO contributions when going from Hf to Ir. At the same time, the HOMO–LUMO gap increases from approximately 2

Table 3: $^{17}$O nuclear shielding constants [$\times(-1)$] in transition metal oxo complexes [a]

| Compound | $\delta$ exp. [b] | BP [c] | BP [d] | BP [e] | B3LYP[d] | HF [d] | MP2 [d] |
|---|---|---|---|---|---|---|---|
| $WO_4^{2-}$ | 129 | 140 | 157 | 138 | 183 | 194 | 21 |
| $MoO_4^{2-}$ | 239 | 216 | 251 | 231 | 289 | 335 | 60 |
| $CrO_4^{2-}$ | 544 | 446 | 508 | 490 | 640 | 1308 | −2173 |
| $ReO_4^-$ | 278 | 278 | 282 | 277 | 339 | 464 | −3 |
| $TcO_4^-$ | 458 | 405 | 421 | 410 | 518 | 819 | −184 |
| $MnO_4^-$ | 939 | 778 | 832 | 821 | 1149 | 7248 | −54485 |
| $OsO_4$ | 505 | 521 | 517 | 503 | 657 | 1295 | −1069 |
| $RuO_4$ | 815 | 740 | 765 | 733 | 1037 | 3330 | −8262 |

[a] Experimental data has been converted to absolute $^{17}$O shieldings based on a value of 290.9 ppm for $\sigma(^{17}O)$ of liquid water at room temperature [62]. All values in the table have been multiplied by $-1$
[b] As compiled in Ref. 62
[c] Scalar relativistic DFT, Pauli operator with frozen core, GIAO. Reference 51
[d] Scalar relativistic ECP, GIAO. Reference 62.
[e] Scalar relativistic ECP, IGLO, paramagnetic term semi-empirically scaled ("SOS-DFT"). Reference 62.

Table 4: Experimental and calulated proton chemical shifts (with respect to TMS, all values multiplied by $-1$) for a number of transition metal hydrides. Data taken from Ruiz–Morales et al., Ref. 81. Nonrelativistic DFT computations (BP functional) except for Re

| | $-\delta(^1H)$/ppm | |
|---|---|---|
| Complex | calc. | expt. |
| $[HCr(CO)_5]^-$ | 6.5 | 6.9 |
| $[HCr_2(CO)_{10}]^-$ | 20.3 | 19.5 |
| $HMn(CO)_5$ | 6.8 | 7.5 |
| $HTc(CO)_5$ | 5.7 | |
| $HRe(CO)_5$ [a] | 5.2 | 5.7 |
| $H_2Fe(CO)_4$ | 7.5 | 11.1 |
| $HCo(CO)_4$ | 5.3 | 10.7 |

[a] quasi–relativistic calculation

to 6 eV. According to Eq. (10a) the increasing denominator should lower the magnitude of the SO contributions. However the binding between the metal and the ligand also changes considerably along the series. While the Hf–C bonds are mostly characterized by $d_\pi - \pi^*_{CO}$ interactions, for Ir–C it is mostly $d_\sigma - \sigma_{CO}$. The SO contributions to nuclear shielding are dominated by the spin–orbit FC mechanism, which is very similar to the one for spin–spin coupling constants [9, 33, 35] and more effectively transfered if the bond has a strong $\sigma$ character. In effect, the magnitude of the matrix elements in the numerator increases more strongly than the denominator increases from Hf to Ir. The trend which is already observed at the scalar relativistic level has been shown to stem from a complex

Table 5: $^{13}$C chemical shifts in 5d transition metal carbonyls, from DFT calculations

| Compound | $\delta$ exp. [a)] | Pauli [b)] | Pauli-SO [c)] | SO-ECP [d)] |
|---|---|---|---|---|
| $[Hf(CO)_6]^{2-}$ | 244 | 228.3 | 234.5 | 228.2 |
| $[Ta(CO)_6]^{-}$ | 211 | 211.8 | 214.8 | 206.0 |
| $W(CO)_6$ | 192 | 197.7 | 196.7 | 188.6 |
| $[Re(CO)_6]^{+}$ | 171 | 183.9 | 176.2 | 173.7 |
| $[Os(CO)_6]^{2+}$ | 147 | 172.4 | 149.5 | 153.9 |
| $[Ir(CO)_6]^{3+}$ | 121 | 153.6 | 125.8 | 130.9 |
| $[Au(CO)_2]^{+}$ | 174 | | 165.3 | 164.0 |
| $[Hg(CO)_2]^{2+}$ | 169 | | 158.2 | 154.0 |

[a)] as compiled in Refs. [52, 79], with respect to TMS
[b)] scalar relativistic Pauli operator (variational procedure employing frozen cores), Reference 82
[c)] Pauli operator including spin-orbit coupling (variational procedure employing frozen cores), Reference 52
[d)] Spin-orbit ECPs, Reference 79

interplay of factors, most notably $\pi$–back–donation from CO [82, 83].

A recent application of the scalar relativistic ZORA methodology has been the calculation of $^{31}$P shifts in the phosphinidenes [84, 85] Cp*(L)M=PAr, with M = Co, Rh, Ir. Good agreement with experimental data was again obtained with a standard non–hybrid functional (BP). The data are listed in Tab. 6 in Sec. 4.2, where the calculated $^{31}$P–$^{31}$P coupling constants are discussed. The ZORA approach was also applied by Webster & Hall in order to compute $^{11}$B chemical shifts for number of substituted tris(pyrazolyl)borate Rh dicarbonyl complexes [86]. Among other results the study reported a correlation between the computed boron shifts, B–H vibrational stretching frequencies and

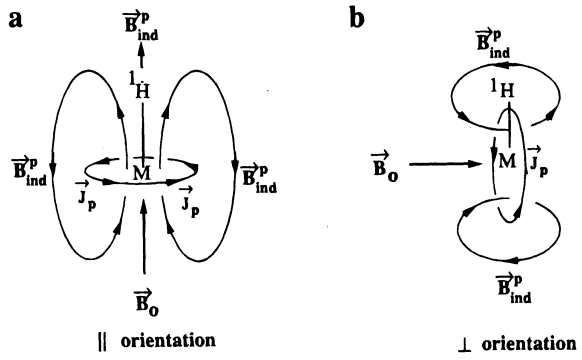


Figure 1: Effect of induced paramagnetic ring currents in low–valent transition metal hydrides. See also Tab. 4. Reprinted with permission from Ruiz–Morales et al., Ref. 81, © (1996) American Chemical Society

the denticity of the tris(pyrazolyl)borate ligand.

Complexes with Mo– and W–phosphorus triple bonds were investigated by Wagener & Frenking [87]. ECPs were used for the metals and the BPW91 non–hybrid functional was applied. Both $^{31}$P isotropic shifts and anisotropies were calculated and compared with available experimental data. Deviations not exceeding 160 ppm were obtained for $\delta(^{31}\mathrm{P})$, with a studied shift range of about 1000 ppm (largest experimental shift: 1364 ppm for [Mo(P)($N_3$N)]). The signs and magnitudes of the parallel and perpendicular components of the shielding tensors were found to be in agreement with experimental data for three of the systems, with deviations between theory and experiment being somewhat larger than for the chemical shifts.

A catalytically important system, methylalumoxane (MAO), has been investigated by Zurek & Ziegler. Computed $^{13}$C and proton chemical shifts of its Zr complexes were used to identify the active and dormant species of this "black box" activator of the dimethylcirconocene homogeneous olefin polymerization catalyst by comparison of the NMR parameters of the proposed species to experimental data (BP non–hybrid functional) [88].

DFT computations (BP non–hybrid functional) of $^{13}$C chemical shifts were recently used to propose a reaction mechanism that leads to di-cubane structures composed of Ti, O, C and alkali metal atoms [89]. $^{13}$C shifts of almost 600 ppm were computed and are in excellent agreement with experimental data.

An early application of DFT NMR methods to systems of biological relevance has been made by Strohmeier et al. [90]. A combined solid state NMR and computational (BLYP non–hybrid functional) study of several metal 5,10,15,20–tertraphenylporphyrin complexes (Zn, Ni, Mg) achieved good agreement with experimental $^{15}$N shielding tensor components. The calculations were also carried out on Zn model systems (phenyl replaced by methyl and H), showing that the $^{15}$N NMR parameters were not significantly affected by the substitutions. A stronger effect was found for the shifts of the substituted carbons, thus a comparison of the $^{13}$C data for the model systems with experiment was not directly possible. The main influence of the metal on the $^{15}$N shielding tensor components was found to be the metal–N distance. Another DFT application to bioinorganic complexes can be found, e.g. in Ref. 91 (heme proteins and model systems, including $^{57}$Fe NMR, B3LYP and BPW91 functionals).

Schreckenbach has investigated ligand chemical shifts in uranium compounds [92–94] (ZORA DFT). Non–hybrid ZORA–DFT computations were not able to reproduce the trends for $^{19}$F shifts of $UF_{6-n}Cl_n$ though the correct magnitudes between 750 and 790 ppm were obtained. Spin–orbit effects were found to be of minor importance for the $^{19}$F shifts. ZORA–DFT computations were successfully applied to fluorine shifts in the $UF_{5-n}(OCH_3)_n$ series. Similar calculations could also well reproduce the trends for $^{17}$O shifts in a number of uranyl complexes. A large–core ECP on uranium in conjunction with the B3LYP hybrid functional did originally reproduce the trends for the $^{19}$F shifts in the $UF_{6-n}Cl_n$ series, but the magnitudes were overestimated by 80 to 270 ppm. A recent re–investigation has shown that small–core ECPs in conjunction with the B3LYP hybrid functional yield results very similar to ZORA PW91 non–hybrid DFT results [95], and the large–core ECP computations have been discredited. It was concluded that the relativistic approximations are not responsible for the failure of the computations to reproduce the experimental trends and it as suggested that a missing treatment of solvent effects might be responsible instead. A chemical shift range of more than 21000 ppm has been predicted for $^{235}$U from the computations in Ref. 93. Unpublished recent calculations by Schreckenbach yielded an even larger chemical shift range of 38000 ppm. However,

Table 6: Experimental and calulated $^{31}$P chemical shifts (with respect to $PMe_3$) and $^2J(^{31}P–^{31}P)$ coupling constants for Cp*(L)M=PAr, with M = Co, Rh, Ir, L = $PR_3$ or CO, Ar = Mes*. Data taken from Termaten et al., Ref. 85. Scalar ZORA DFT computations (BP functional) on model complexes with L = $PH_3$ or CO, Ar = H, and Cp instead of Cp* where appropriate

| | $\delta(^{31}P)$/ppm | | $^2J(^{31}P–^{31}P)$/Hz | |
|---|---|---|---|---|
| Complex | calc. | expt. | calc. | expt. |
| (*E*)–Cp($PPh_3$)Co=PMes* | 903 | 867 | 207 | 76 |
| (*E*)–Cp*($PPh_3$)Rh=PMes* | 894 | 868 | 171 | 59 |
| (*Z*)–Cp*($PMe_3$)Rh=PMes* | 942 | 953 | 30 | 19 |
| (*E*)–Cp*($PPh_3$)Ir=PMes* | 729 | 687 | 216 | 102 |
| (*Z*)–Cp*($PMe_3$)Ir=PMes* | 768 | 727 | 21 | 18 |
| (*Z*)–Cp(CO)Co=PMes* | 1044 | 1047 | | |
| (*Z*)–Cp(CO)Ir=PMes* | 844 | 805 | | |

there are no experimental data available for comparison.

A number of additional DFT applications are reviewed in Refs. 1, 2 and 3, 96. In many cases, reasonable results were obtained with non–hybrid density functionals. For 5d metal complexes it can be necessary to include spin–orbit coupling, though the trends for ligand shifts are often reproduced already at the scalar relativistic level (similar to the systems in Tab. 5). Interestingly, it will be demonstrated below that the calculation of metal shielding constants is very sensitive to the choice of the functional and that the hybrid types tend to perform much better, at least for the 3d metals. Thus, it is either a very general systematic error compensation, or that the ligand shifts are rather insensitive to the approximations in the most common functionals, which permits to obtain reasonably accurate ligand shifts for transition metal complexes.

### 4.2 Computations of ligand–ligand spin–spin coupling constants

There are at present not very many studies of ligand–ligand coupling constants in transition metal complexes available. One reason is perhaps that the interest is often in coupling constants between nuclei that are separated by more than one bond, for instance ligands that are both bound to the metal but not to each other. Two–bond coupling constants appear to be more difficult to calculate accurately. Another reason might be that for the DFT calculation of spin–spin coupling constants, generally a coupled perturbed problem has to be solved which results in a higher computational cost than solving an uncoupled problem (as it is the case for nuclear shielding with non–hybrid DFT). The number of program codes that have not just the FC term implemented but also the OP, OD, or even the SD term is also smaller compared to the many available codes for nuclear shielding.

Among the available examples in the literature, two–bond $^{31}$P–$^{31}$P coupling constants $^2J$(P–P) have been studied using different methods. Very recently, the scalar relativistic ZORA DFT method has been applied to the calculation of $^2J$(P–P) in organometallic systems of the type Cp*(L)M=PAr, with M = Co, Rh, Ir, L = $PR_3$ or CO; and Ar = Mes* [85]. The computations were based on model systems with R = H and Ar = H. The results are listed in Tab. 6. Though the $^{31}$P chemical shifts for the model systems which were already discussed in Sec. 4.1 are in good agreement with the experimental

data, the results for the $^2J$(P–P) are less favorable. Two trends are reproduced by the computations. First, the $^2J$(P–P) for the ($E$) isomers are consistently larger than for the corresponding ($Z$) forms. Second, the trend for the magnitude of $^2J$(P–P) is Ir > Co > Rh for the ($E$)-Cp*($PR_3$)M=PAr systems. This is an indication that the influence of the metal is correctly described in the calculations. It is likely that the deviations between the calculations for the model complexes and the experimental data for $^2J$(P–P) are caused by electronic effects from the model phosphorus ligands rather than deficiencies in the methodology. Because of the known sensitivity of spin–spin coupling constants to basically all approximations in the computational model it might be necessary to carry out calculations on the same systems that were experimentally studied (and have large bulky ligands on the P's).

$^{31}$P–$^{31}$P coupling constants in group VI metal carbonyl phosphines $M(CO)_4(PH_3)_2$, M = Cr, Mo, W, have been investigated by Kaupp [1, 97], employing a scalar relativistic ECP on the metal. The results that were obtained with a number of different density functionals are graphically displayed in Fig. 2. It can be seen that there is a significant influence from the specific type of non–hybrid functional that has been applied, testifying to the sensitivity of the investigated properties with respect to the quality of the electronic structure. It can also be seen that the $^2J(^{31}$P–$^{31}$P) are noticeably

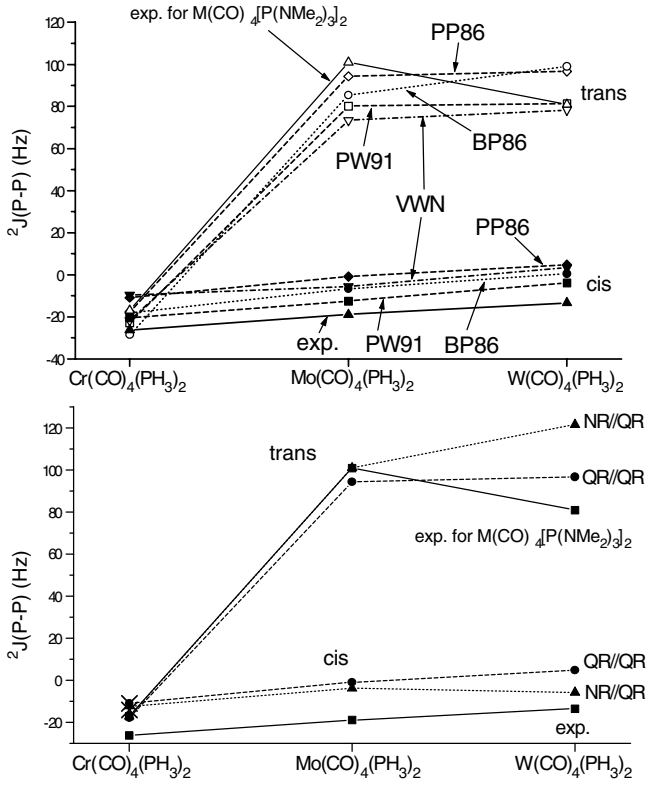


Figure 2: Influence of the choice of the XC potentials and of relativistic effects on the $^{31}$P–$^{31}$P two–bond coupling constants in *cis*– and *trans*–$M(CO)_4(PH_3)_2$, M = Cr, Mo, W. Graphics courtesy of M. Kaupp. The data was published in Ref. 97

influenced by relativistic effects (about 20 Hz for the *trans* tungsten complex), with the relativistic computations being closer to experiment than the nonrelativistic ones. The trends for the *cis* and *trans* series are well reproduced by this approach and could be related to a few characteristic orbital contributions. The reader is referred to Refs. 35, 97 for further details.

Lichtenberger has recently investigated the Si–H coupling constant in the organometallic complex $(\eta^5\text{–}C_5H_5)(CO)_2MnHSiCl_3$ [98]. The scalar relativistic ZORA–DFT method (BP non–hybrid functional) has been employed. A MO based analysis along with a comparison of calculated and experimental Si–H coupling constants has been applied to shed some light on the type of bonding between Si and H and the Mn center and the question whether there is direct bond between Si and H. For $HSiCl_3$, the experimentally determined magnitude of the Si–H coupling constant is 370 Hz (calculated: −338 Hz) but 54.8 Hz in $(\eta^5\text{–}C_5H_5)(CO)_2MnHSiCl_3$ (calculated as −38 Hz for an optimized geometry and −46 Hz when using the experimental Mn–Si distance). The negative sign of the Si–H coupling constant in $HSiCl_3$ is hereby due to the negative magneto–gyric ratio of the Si nucleus. In comparison, the Si–H coupling in $(CO)_4Fe(H)(SiCl_3)$ is positive (expt.: 21.7, calculated: 16 Hz) and interpreted as a two–bond coupling without a direct Si–H bond contribution. In Ref. 98, the case of $(\eta^5\text{–}C_5H_5)(CO)_2MnHSiCl_3$ has consequently been described as an intermediate between these two extremes, in agreement with a 75% reduction of the Si–H bond population in the Mn complex as compared to $HSiCl_3$.

A three-bond $^{13}C\text{–}^{13}C$ coupling constant has been investigated by Autschbach & Ziegler for the complex $[(NC)_5Pt\text{–}Tl(CN)]^-$. This and related complexes will be discussed in more detail in the following sections. For the labeling of the carbon atoms see Fig. 8. Based on scalar relativistic ZORA computations (VWN functional), the $C^A\text{–}C^B$ coupling constant was determined as 24 Hz (in the most accurate computational model which included SO coupling as well as coordination of the Tl center by $H_2O$). The experimental value [99] is 30 Hz. The three–bond $C^C\text{–}C^B$ coupling, on the other hand, is extremely small. It is noteworthy that the combined contributions due to the SD terms as well as SO effects on $J(C^A\text{–}C^B)$ in the calculations amounted to as much as 4 Hz (∼17% of the total three–bond coupling), resulting from the fact that the coupling is mediated by the strongly delocalized metal–metal and metal–carbon bonds, with a significant influence of relativistic effects in the metals' valence shells.

A Hartree-Fock and MP2 study of $^1H\text{–}^2H$ (H–D) coupling constants in complexes of the type $[(\eta^2\text{-}H_2)Os^{II}(NH_3)_4L]$, with L being a ligand *trans* to $H_2$, by Hush et al. in 1994 did yield magnitudes for the $J$(H–D) that were similar to the experimental ones, but the trends for different ligands L were not reproduced correctly [101]. Large differences were further found between the Hartree-Fock and MP2 values for $J$(H–D), along with non–systematic sign changes. Only the FC mechanism was considered as a finite perturbation in this work (a coupled Hartree–Fock implementation of the FC term was also reported). A scalar relativistic ECP was used for Os. In 1996, Hush et al. re–investigated the same set of complexes, this time employing DFT [100] (BLYP non–hybrid functional). Figure 3 displays the agreement between experimental and theoretical data which is much more favorable than what was previously obtained with the Hartree-Fock and MP2 methods. The authors attributed this success to a more accurate description of electron correlation effects at the DFT level as compared to MP2. It was further found a strong correlation between the calculated $J$(H–D) and the strength of the Os–$H_2$ interaction as well as a correlation between $J$(H–D) and the H–D internuclear distance in the complexes.

### 4.3 Computations of metal nuclear shieldings

It has turned out that the computation of metal nuclear shieldings and chemical shifts is much more difficult than the calculation of ligand shifts which were discussed above. It appears that metal shieldings are more sensitive to the quality of the computed electronic structure and consequently larger influences due to the XC potential are observed. Regarding the 3d metals, it has turned out that hybrid functionals appear to be particularly well suited for NMR computations of the metal shielding constants. This cannot be easily extrapolated to all of the transition metals, though, since counter examples are known for which non–hybrid functionals perform better. On the other hand, some 4d metals have most successfully been treated with hybrid functionals.

Figure 4 displays calculated vs. experimentally observed $^{103}$Rh chemical shifts for 13 complexes [3]. The nonrelativistic DFT computations (B3LYP hybrid functional) were obviously able to achieve excellent agreement with experiment. In comparison, a non–hybrid functional achieved also a linear relation between the calculated and the experimental value, but the slope of the linear fit was 0.9 instead [1, 102]. $^{99}$Ru chemical shifts have also been calculated more accurately with the B3LYP functional [103]. It has further been concluded from the success of these and other nonrelativistic computations on 4d metal shifts [1, 3] that relativistic effects on the shielding tensor, though known to be quite substantial, almost completely cancel when the chemical shifts are evaluated. These findings indicate that (at least the scalar) relativistic effects on shielding constants for 4d (and lighter) metals are almost exclusively originating in contributions from the core orbitals, which are not substantially altered by the chemical environment of the metal. It should be noted that these considerations apply if

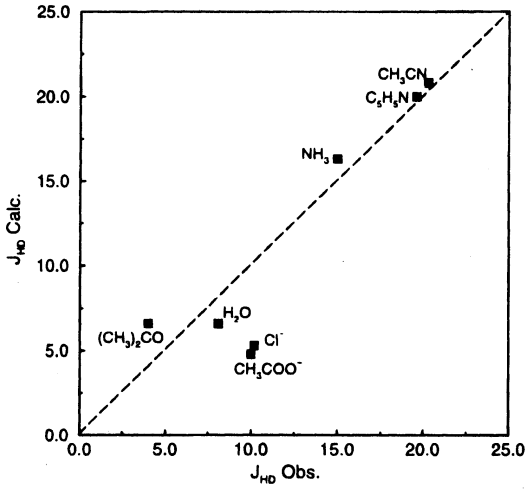


Figure 3: Calculated vs. experimental $^1$H–$^2$H (H–D) spin–spin coupling constants in the complexes $[(\eta^2\text{-}H_2)Os^{II}(NH_3)_4L]$, from DFT calculations (BLYP). The ligand L is indicated in the graphics. The dashed line does not represent a fit but indicates where $J_{HD}$Calc. = $J_{HD}$Obs. Reprinted with permission from Ref. 100, © (1994) American Chemical Society

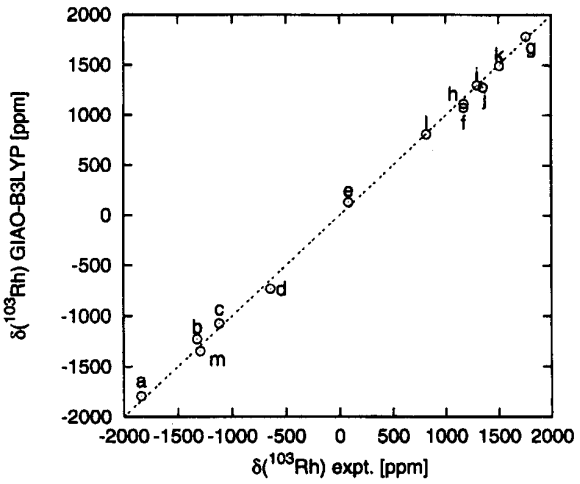


Figure 4: Calculated vs. experimental $^{103}$Rh shifts for a number of Rh complexes. Reprinted with permission from Bühl et al., Ref. 3, © (1999) John Wiley & Sons, Inc.

the metal is the only heavy atom in the complex. If there are heavy ligand atoms present in particular the SO effects on the metal shift originating from a heavy neighbor atom should be considered. In a Hartree-Fock study of neighbor atom induced spin–orbit contributions to Nb and Ti chemical shifts it was argued, on the other hand, that this SO effect is canceled by competing effects in the metal's valence shell [104], which appears to be rather typical for early transition metals. For 5d metals the situation is, in general, different and relativistic effects on the metal shielding can be induced by the metal itself. This point will be discussed further below.

It is a typical observation that for many 4d and 5d metals non–hybrid functionals perform reasonably well as, sometimes better than, hybrid functionals. In the case of $^{95}$Mo chemical shifts, the non–hybrid BPW91 functional yields in fact superior results to B3LYP [3]. Bryce & Wasylishen have recently found excellent agreement for the $^{95}$Mo (and $^{13}$C) chemical shift with solid–state NMR data for the mesitylenetricarbonylmolybdenum(0) piano–stool complex. The ZORA DFT calculations (BP non–hybrid) functional yielded $-1873$ ppm, as compared to the experimental value of $-1885 \pm 2$ ppm. A non–relativistic DFT calculation employing the B3LYP hybrid functional yielded $-460$ ppm instead. It is thus of importance to carefully investigate the performance of various functionals before drawing general conclusions from DFT computations on 4d metal chemical shifts.

For the 3d metals there is now much experience showing that non–hybrid functionals are not very reliable for metal chemical shift computations, but that B3LYP and other hybrid functionals perform very well. Bühl has in 1997 investigated (along with Rh) the illustrative case of $^{57}$Fe chemical shifts [102]. The slopes of linear fits of the calculated to the experimental data for nine iron complexes were 0.65 for the non–hybrid BPW91 functional, but an excellent 0.97 was obtained with the B3LYP hybrid functional. The BPW91 results for ferrocene were particularly poor (657 ppm vs. an experimental value of 1532), whereas B3LYP achieved almost perfect agreement with experiment (1485 or 1525 ppm, depending on the basis set). Similar results were recently reported for eleven $^{55}$Mn chemical

shifts [105] (slopes of 0.72 and 0.99, respectively). Pioneering nonrelativistic DFT studies of $^{59}$Co chemical shifts have also concluded that the B3LYP and other hybrid functionals are able to achieve a good agreement with experiment [106, 107], but that the non–hybrid BLYP functional leads to less satisfactory results [106]. On the other hand, the first systematic DFT study of transition metal shifts concluded that $\delta(^{51}\mathrm{V})$ is equally well described by hybrid and non–hybrid functionals [108], with mean errors of about 3% of the investigated chemical shift range of 3500 ppm. Figure 5 displays the performance of the B3LYP functional for a large number of calculated 3d and 4d metal shifts, including some of the previously discussed cases. Except for Mo, the overall performance of the hybrid DFT calculations is very satisfactory.

The infamous case of the $^{57}$Fe chemical shift in ferrocene has later been studied in very detail by Schreckenbach [51]. Compared to the reference (iron pentacarbonyl) $^{57}$Fe in ferrocene is stronger shielded due to a smaller magnitude of the negative paramagnetic contribution $\sigma^p$. With the non–hybrid functionals the magnitude of $\sigma^p$ is strongly underestimated, which results in a too small chemical shift. The influence of a hybrid functional is threefold. On the one hand, it was found that the HOMO–LUMO gap approximately doubled due to the admixture of Hartree–Fock exchange in the XC potential. However, according to Eq. 9a one would naively expect that this causes a reduction of the magnitude of $\sigma^p$ and thus an even smaller chemical shift. At the same time, the hybrid functional causes the orbital shapes to alter significantly, which was found to result in much larger matrix elements in the numerator of the paramagnetic term in (9a). A third factor is the coupled contribution from Hartree–Fock exchange, which was also found to increase the magnitude of $\sigma^p$. The

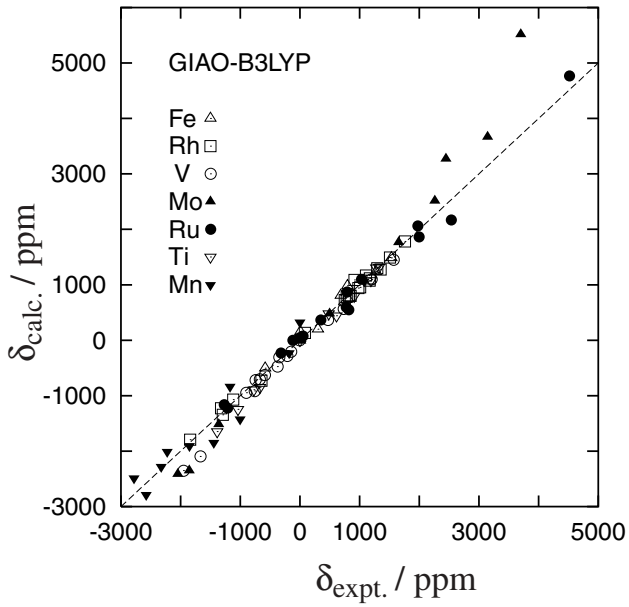


Figure 5: DFT computed metal NMR chemical shifts (B3LYP hybrid functional) for a large number of inorganic and organometallic transition metal compounds. The dashed line is not a fit but indicates where $\delta_{\mathrm{calc}} = \delta_{\mathrm{expt.}}$. Graphics courtesy of M. Bühl. See Ref. 5 for further details

previously mentioned SOS–DFT approach only affects the energy denominators in Eq. (9a) and was consequently found to yield an even smaller chemical shift for ferrocene than a standard uncoupled method [102] (133 ppm, expt.: 1532). The findings by Schreckenbach are probably transferable to other 3d transition metal systems.

$^{113}$Cd chemical shifts have recently been calculated for a number of bioinorganic complexes [109, 110]. The nonrelativistic DFT method employed the B3PW91 hybrid functional. The agreement with experimental data from solid state NMR was satisfactory (deviations of less than 30 ppm on a shift range of about 400 ppm) for most of the complexes. For Cd–alaninate and Cd–glycylglycinate, the differences were larger (74 and 48 ppm, respectively.). Individual tensor components were also studied and compared well with experiment. An earlier computational investigation of Cd chemical shifts was carried out on model systems for the active site of the Cd(II) substituted enzyme phosphotriesterase [111] (B3LYP hybrid functional). The computed pronounced dependence of the Cd shielding constant on the metal's coordination number was used in conjunction with information from X–ray diffraction data to determine which of a number of computed equilibrium model structures of similar energy is likely to correspond to the enzyme's structure in solution.

For further data on DFT computations of 3d and 4d metal shieldings the reader is referred to Refs. 1, 3 and 5.

When 5d metals are to be included in a study of metal shifts a relativistic NMR approach should be used. There are cases in which the heavy atom's (HA) effects on its own shift (this has been coined a HAHA effect [112]) approximately cancel, but this cannot not always be expected. The reason for this lies in the fact that for the heavy 5d metals relativistic effects have a very substantial influence on the way it binds to its ligands [37] (along with bond–length contractions of up to several 10 pm). This alters qualitative features of the bond, for instance the metal 6s/5d contributions in metal–ligand bonds. Since the chemical shift with respect to a reference compound results precisely from the different bonding environment, relativity will have an effect on the chemical shift as soon as its acts strongly — and noticeably differently — in the metal–ligand bonds of the reference and the probe. This is not so much the case for the 4d metals for which relativistic effects on the chemical bond are much smaller and thus the most prevalent relativistic contributions are from the core shells that cancel between probe and reference. As an example, Fig. 6 displays the $^{199}$Hg shifts of Me–Hg-X, X = Cl, Br, I, with respect to the $HgMe_2$ reference, excluding or including spin–orbit contributions in the shielding constants. The DFT results are in reasonable agreement with experiment, though the trend is not well reproduced. In comparison, the Hartree–Fock results, though close to the DFT values when SO coupling is excluded, yield a much too large chemical shift range for the series. It is obvious, though, from both DFT and Hartree-Fock computations that there are very considerable spin–orbit relativistic effects on the $^{199}$Hg chemical shift that need to be properly described in a computation. The scalar relativistic contributions to $\delta$(Hg) are also substantial. A larger set of computed Hg chemical shifts is compiled in Refs. 6 and 7 which allows the same conclusion.

Scalar relativistic (Pauli operator, BP functional) frozen core computations of the metal shifts in group VI oxides $MO_4^{2-}$ and carbonyls $M(CO)_6$ showed that scalar relativistic effects on the metal shift strongly increase from the 3d to the 5d metals [51]. For the carbonyl complexes, for instance, $\delta(^{95}\mathrm{Mo})$ was only reduced by 10 ppm due to relativistic effects, whereas the corresponding change in $\delta(^{183}\mathrm{W})$ was found to be $-435$ ppm, leading to a much better agreement with experiment. These and further computational data on $^{183}$W chemical shifts are collected in Tab. 7. Some Hartree-Fock data are also listed for comparison. The metal chemical shifts of the tetroxo-metallates listed in Tab. 3 have

Table 7: $^{183}$W chemical shifts, from DFT and Hartree–Fock computations

| Compound | $\delta$ exp. [a] | DFT vPSC [51] | | DFT vPSCSO [113] | DFT ZORA [113] | HF DKH2/vPSO [114] [b] | |
|---|---|---|---|---|---|---|---|
| | | nrel | rel | rel | rel | nrel | rel |
| $W(CO)_6$ | -3446 | -4075 | -3703 | -3306 | -3876 | | |
| $WF_6$ | -1121 | | | -107 | -630 | -1795 | -1135 |
| $WCl_6$ | 2181 | | | 1773 | 1932 | 2266 | 2686 |

[a] with respect to $WO_4^{2-}$, as compiled in Ref. [113]

[b] Scalar relativistic DKH2 approach with Pauli spin–orbit operator, reported in [114] with respect to $WF_6$

been studied mainly with relativistic effects in mind. The DFT ZORA and vPSCSO method were compared and ZORA has emerged as the more accurate one. Unfortunately, the oxygen shieldings were not reported for comparison.

A larger number of tungsten chemical shifts were computed with the relativistic ZORA and the vPSCSO approaches in Ref. 113. Pb shifts were also studied in this work. A rather small mean error of 3% of the investigated $^{183}$W chemical shift range of 7000 ppm was obtained from the ZORA computations (the Pauli approach yielded 6% error). Using the same methodology, the $^{183}$W nucleus in the exotic species $WAu_{12}$ has recently been predicted to be exceptionally strongly shielded, resulting in a chemical shift of about −13000 ppm [115]. No experimental data is yet available in order to confirm

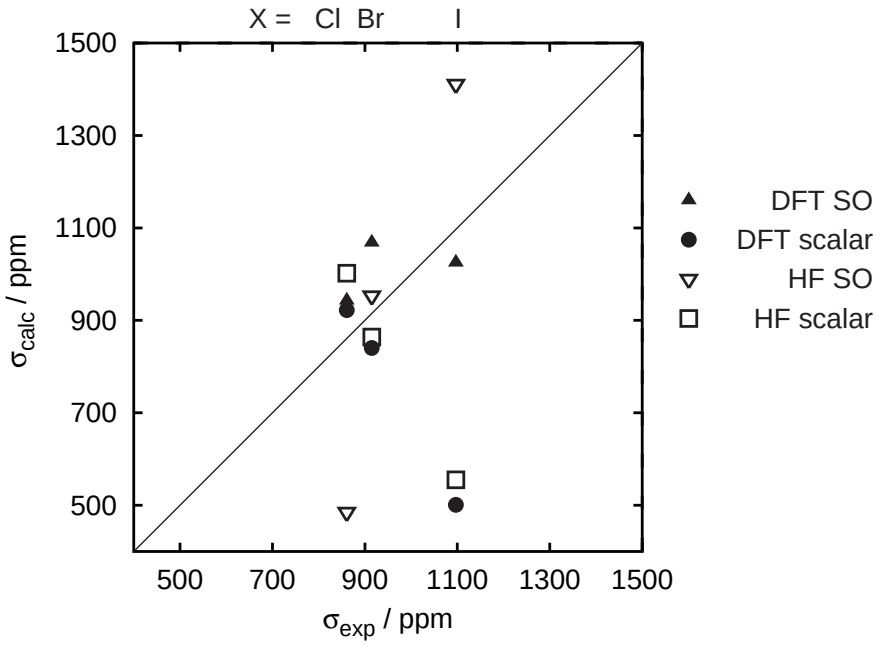


Figure 6: $^{199}$Hg chemical shifts (with respect to $HgMe_2$, in ppm) for MeHgX, X = Cl, Br, I, from ZORA DFT (PW91 non–hybrid functional) and DKH2 Hartree–Fock computations. Data taken from Refs. 43 and 48

this finding.

The ZORA DFT approach was further applied by Gilbert & Ziegler to the computation of $^{195}$ Pt chemical shifts [116]. The accuracy of the result was less favorable, with a mean error of about 10% of the investigated chemical shift range. A detailed analysis of the result by means of the HOMO–LUMO gap and the magnitude of the contributing matrix elements was carried out. As in previously mentioned cases, the HOMO–LUMO gap alone would cause opposite trends for $\delta$(Pt) along a series of complexes (for instance for series of Cl, Br, I ligands), but is overcompensated by changes in the matrix elements (the numerator of Eq. (9a)).

The reader is referred to Refs. 6 and 7 for further examples of relativistic NMR metal shieldings computations.

Now that computationally efficient DFT methods for metal chemical shifts are available and established, applications start to appear in which comparisons of computational results for isolated metal complexes with experimental (usually solution) data is questioned and more elaborate approaches are taken. With the known sensitivity of the shielding tensor in mind, it is natural to include effects from solvation into the computations, and to consider vibrational effects and temperature. Applications to transition metal chemical shifts have been carried out by Bühl et al. [12–14, 96, 117]. The protocol consisted of performing ab–initio molecular dynamics [118] simulations (Car–Parrinello or Born–Oppenheimer type) of the complexes at a given temperature, including solvent molecules where necessary, and averaging NMR computational results (DFT, B3LYP hybrid–functional) for a number of snapshots along the trajectory. For vanadate complexes in aqueous solution [96, 117] and the permanganate ion [12] differences between the averaged chemical shift $\delta_{av}$ and the one obtained from a single computation at the equilibrium structure $\delta_e$ did not exceed 50 ppm, which is rather insignificant when compared to the chemical shift ranges for these metals. On the other hand, for the $^{57}$Fe chemical shift in $[Fe(CN)_6]^{4-}$, $\delta_{av}$ with respect to iron pentacarbonyl was found to be more than 1500 ppm smaller than $\delta_e = 4120$ ppm, based on simulations including water molecules [14]. This included a $-246$ ppm change of the reference shielding constant due to thermal averaging. The experimental chemical shift is 2455 ppm. Without adding the solvent, $\delta_{av}$ was even larger than $\delta_e$ which thus increased the difference between the computed and the experimental value by another 455 ppm. The final results of $\delta_{av} = 2593$ ppm based on the simulations with solvent is in excellent agreement with the experimental value of 2455 ppm when taking the enormous thermal and solvent effects into consideration. These effects were rationalized by the exceptional sensitivity of $\delta(^{57}\mathrm{Fe})$ to the metal–ligand bond distances and the high charge of the complex. The study has later been extended to investigate the strong shielding of $^{57}$Fe ($\delta = 2004$ ppm) in $[Fe(CN)_5NO]^{2-}$ compared to $[Fe(CN)_6]^{4-}$ ($\delta = 2455$ ppm) [13]. For the former, the calculated $\delta_{av}$ was found to be in good agreement with experiment (about 1997 and 2076 ppm upon inclusion of solvent, with the Car–Parrinello and Born–Oppenheimer simulations, respectively) and differed from $\delta_e$ by about 250 ppm.

Solvent effects on $^{199}$Hg chemical shifts were computationally investigated by Wolff et al. [43] already in 1999. Here, explicit solvent molecules were included in relativistic ZORA DFT NMR computations (PW91 non–hybrid functional) in order to account for the direct metal–solvent interaction occurring in solution. The computations could correctly reproduce the sign and magnitude of solvent changes of $\sim 10^3$ ppm which were already known from NMR measurements for a long time. The geometry change (bending) of linear $HgX_2$ due to solvent complexation was found to be of similar importance as the direct electronic effect of the solvent.

### 4.4 Computations of metal–ligand and metal–metal spin–spin coupling constants

When discussing computational results for spin–spin coupling constants it should be kept in mind that this molecular property is at least as, often even more, sensitive to the approximations in the computational model as nuclear shieldings (geometries, basis sets, XC potentials, environment, etc.). Thus, an agreement with experiment within some 10% margin must be classified as excellent for a molecule the size of a typical (even small) transition metal complex. 20% errors are often still considered acceptable since for more difficult cases it is sometimes even a challenge to calculate the correct sign of the coupling constant. In addition, relativistic effects can be enormous for 5d metals and significant even for the 3d metals. This is among the reasons why many DFT studies of metal–ligand and metal–metal coupling constants have focussed on relativistic effects.

First–principles theoretical metal–ligand (M–L) one–bond coupling constants for 3d metal complexes were first reported as part of the validation study of Dickson & Ziegler's nonrelativistic DFT implementation [69] (VWN non–hybrid local functional). The reduced M–C coupling constants for the carbonyls $[V(CO)_6]^-$, $Fe(CO)_5$ and $[Co(CO)_4]^-$ were calculated as 127, 213 and $353 \cdot 10^{19} T^2 J^{-1}$, as compared to experimental values of 146, 239 and $400 \pm 20$, respectively (averaged value for equatorial and axial carbons for the iron carbonyl). The approximately 15% underestimation of the coupling constants was attributed to approximations in the density functionals, the missing SD mechanism, basis set limitations, geometries, neglected vibrational effects, or a combination of all these. It is also likely that missing relativistic corrections on the M–L coupling are of the order of 10% and thus might account for most of the deviations between theory and experiment.

A larger set of samples was later studied by Khandogin & Ziegler [119], employing the same program code (BP non–hybrid functional). The results are collected in Tab. 8. It can be seen that the coupling constants for the complexes $[V(CO)_6]^-$, $Fe(CO)_5$ and $[Co(CO)_4]^-$, are only slightly affected by the different choice of functional, since the Dickson & Ziegler 1996 results are almost exactly reproduced. [2] It should be noted that differences due to the choice of the XC potential are usually somewhat larger because of the sensitivity of nuclear spin–spin coupling constants. Due to the fact that the FC mechanism was implemented in form of a finite perturbation, the ligand nucleus had to be chosen as the "perturber". Otherwise the procedure would not yield reliable results. (In a properly implemented analytical scheme the result does / must not depend on which nucleus is chosen as the perturbing one.) The OP term was treated in an uncoupled manner, similar to the paramagnetic portion of $\boldsymbol{\sigma}_A$ in non–hybrid DFT schemes. It was found that this approach resulted in reasonable agreement with experiment in almost all cases, with permanganate being the notable exception. This complex was found to be difficult because the small magnitude of the coupling constant is caused by a large, positive FC term which is almost completely cancelled by a negative OP contribution. Accordingly, the relative error in the calculation is large. Substantial OP contributions were also seen for the M–F coupling constants. Generally, when one (or both) of the coupled atoms has many lone pairs, the OP term in $\mathsf{K}_{AB}$ can be expected to be large. For instance, it dominates the coupling constants for diatomics of the p–block of the periodic table [46, 120].

Khandogin & Ziegler have further performed an extensive analysis of the computational results for the FC mechanism. It was found that only MOs with s–type contributions from both the metal and

[2] It is not explicitly stated in Ref. 69 which functional has been used. However, it is noted that for the set of small molecules the "LDA" results compare well with theoretical data in the literature. It is thus reasonable to assume that the VWN functional was employed throughout

Table 8: Reduced one–bond metal–ligand spin–spin coupling constants for some transition metal complexes, in $10^{19}T^2J^{-1}$. DFT computations (BP non–hybrid functional) employing all–electron Slater–type basis sets for the 3d metal M–C and M–O couplings, Slater–type frozen–core basis sets for the metals in all other cases. Data taken from Khandogin & Ziegler, Ref. 119

| Complex | Coupling $K$ | calc.[a] | expt. |
|---|---|---|---|
| $V(CO)_6^-$ | V–C | 129 | 146 |
| $Fe(CO)_5$ | Fe–C [b] | 216 | 239 |
| $Co(CO)_4^-$ | Co–C | 348 | 400±20 |
| $Nb(CO)_6^-$ | Nb–C | 226/262 | 319 |
| $Mo(CO)_6$ | Mo–C | 251/293 | 344 |
| $Rh(CO)_4^-$ | Rh–C | 604/713 | 778 |
| $W(CO)_6$ | W–C | 547/816 | 997 |
| $VO_4^{3-}$ | V–O | 150 | 144 |
| $CrO_4^{2-}$ | Cr–O | 104 | 108 |
| $MnO_4^-$ | Mn–O | 29 | 75 |
| $MoO_4^{2-}$ | Mo–O | 355/346 | 380 |
| $TcO_4^-$ | Tc–O | 408/403 | 350 |
| $ScF_6^{3-}$ | Sc–F | 49 | 59.6 |
| $TiF_6^{2-}$ | Ti–F | 51 | 53.2 |
| $VF_6^-$ | V–F | −27 | 29.7 |
| $NbF_6^-$ | Nb–F | 96/74 | 125 |
| $WF_6$ | W–F | 260/84 | 86.6 |
| $V(PF_3)_6^-$ | V–P | 466 | 399 |
| $Cr(PF_3)_6$ | Cr–P | 460 | 386 |
| $Co(PF_3)_4^-$ | Co–P | 861 | 1063 |
| $Ni(PF_3)_4$ | Ni–P | 903 | 1080 |
| $Nb(PF_3)_6^-$ | Nb–P | 798/978 | 883 |
| $Mo(PF_3)_6$ | Mo–P | 780/948 | 879 |
| $Pt(PF_3)_4$ | Pt–P | 2981/3770 | 6215 |

[a] Nonrelativistic/scalar–relativistic (vPSC) DFT calculations for the 4d and 5d metals (nonrelativistic spin–spin coupling perturbation operators). Nonrelativistic results for 3d metals
[b] Average calculated value for equatorial and axial carbons ((3 eq. + 2 ax.)/5)

the ligand contributes to the FC portion of $K$(M–L). This can in turn be interpreted as the spin–spin coupling constant being a valence property, since core–orbitals do not have large values at both nuclei. Lone–pair orbitals do hardly contribute directly for the same reason, but they can have important indirect effects, as noted above. Some emphasis was further placed on relativistic effects, since the nonrelativistic results for some of the 5d metal complexes drastically deviated form the experimental data. See, for instance, the entries for $WF_6$, $W(CO)_6$ and $Pt(PF_3)_4$ in Tab. 8. The scalar relativistic frozen–core computations (along with nonrelativistic operators implemented in the spin–spin coupling code) did not yield a sufficient improvement over the nonrelativistic results (except for $WF_6$) and it was concluded that a more sophisticated treatment is necessary. It was also shown that, though the

AO matrix elements in particular of the FC operator always increased relativistically, the relativistic effect on the coupling constant might be positive or negative due to different signs of individual contributions. The same authors have subsequently tried to extend the frozen–core scalar relativistic Pauli approach in order to yield improved relativistic values for the FC matrix elements [53]. This was tested on a number of 5d metal complexes (including $WF_6$, $W(CO)_6$ and $Pt(PF_3)_4$), but with limited success regarding the agreement with experiment. This work also contains a study of the *trans* effect in square planar Pt complexes and its relation to the one–bond Pt–P coupling constants.

Significant progress in the field of relativistic DFT spin–spin coupling computations involving one heavy metal nucleus, or even two metal nuclei, has been made recently due to the availability of the ZORA DFT approach [45, 46]. For the late 3d metals, relativistic effects can roughly be estimated to be of the order of 10% for a metal–ligand coupling [121]. For the 5d metals they might amount to 100% or more of a respective nonrelativistic result. Up to an order of magnitude increase might be expected for a coupling constant between two 5d metals. These estimates are based on relativistic scaling factors for the FC term [121, 122] and serve only as an order–of–magnitude guideline, and only in case the coupling constants are not dominated by one of the other mechanisms (most notably OP). A number of computations have so far demonstrated that relativistic correction factors for the FC mechanism are of limited use. In particular for 5d metals a scaling of nonrelativistic AO contributions to the FC mechanism does often not yield correct results as the relativistic effects on the FC matrix elements might be quenched or amplified by relativistic effects on the chemical bonds.

Figure 7 displays a comparison of scalar ZORA DFT results (VWN non–hybrid local functional) with experimental data for the one–bond metal–ligand coupling constants of a number of complexes containing W, Pt and Hg (a few data points for Pb are also included). The result for $Pt(PF_3)_4$) is indicated and should be compared to the nonrelativistic value in Tab. 8. An increase of more than 100% of the nonrelativistic value brings the computed result in excellent agreement with experiment [45]. The case of $Hg(CN)_2$ is similar, with the nonrelativistic Hg-C coupling being about 40% of the experimental value. However, the scalar ZORA DFT computation on $Hg(CN)_2$ yields "only" $443 \cdot 10^{20}$ $T^2J^{-1}$, but the experimental value in methanol is 577.8. Spin–orbit corrections are not responsible for the deviation (they amount to about $-18 \cdot 10^{20}$ $T^2J^{-1}$). It was found that up to 4 methanol molecules had to be included in the computations [124]. Their coordination to the Hg center increased the coupling constant by another $135 \cdot 10^{20}$ $T^2J^{-1}$, yielding almost exactly the experimental value. It was found that such direct solvent coordination resolved most of the deviations between calculated and experimental values that had remained in the original study, Ref. 45. Thereby, only complexes with open coordination sites have to be considered, such as the linear Hg and the square planar Pt complexes. An analysis of the effect [124] indicated that it might be caused by a small amount of charge donation from the solvent into the metal–ligand bonds. The effect is stronger the more nucleophilic the solvent is and the more solvent molecules are coordinated to the heavy metal. Generally, it was found that upon completion of the first coordination sphere of the metal by solvent molecules, agreement with experiment becomes at least satisfactory, often excellent. Even "inert" solvents such as chloroform can cause a substantial solvent effect.

An even more pronounced example of solvent effects on spin–spin coupling constants is seen to govern the NMR spectrum of the complexes $[(NC)_5Pt–Tl(CN)_n]^{n-}$, $n$ = 0, 1, 2, 3 (**I–IV**) and the related system $[(NC)_5Pt–Tl–Pt(CN)_5]^{3-}$. See Fig. 8. A preliminary computational ZORA DFT investigation indicated that at least 50% of the huge magnitude of the Pt–Tl coupling constant (expt.: 57 kHz) of the $n = 1$ system **II** is due to coordination of Tl by solvent molecules (water) [125]. This was

also the first DFT study of a coupling constant between two heavy metals. A recent study of the whole series has confirmed the large solvent effects and shown that their influence on the $n = 0$ system **I** is even larger [126]. Thereby, it was also found that bulk solvent effects need to be included in the computations as well, and that the simultaneous application of both an a continuum solvent model (COSMO [127,128]) and an improved XC potential (SAOP) [32,129] yields good agreement with the experimental values for the Pt–Tl coupling constant. The computational results are displayed in Fig. 9. The metal–ligand coupling constants for these systems have also been studied in Ref. 126, with similar success. The Tl–C coupling constants are very strongly influenced by the solvent, whereas the Pt–C coupling constants are less affected though some improvement is obtained from considering the solvent. Solvent coordination was further found to be mainly responsible for the unintuitive relative magnitudes of $^1J$(Tl–C) and $^2J$(Tl–C) for complex *II* [125], with the latter being more than 3 times larger than the former.

The magnitudes of $^{195}$Pt–$^{195}$Pt coupling constants were the subject of a theoretical investigation in Ref. 131. It has long been known experimentally that Pt–Pt coupling constants in chemically closely related dinuclear complexes can differ by an order of magnitude — with no obvious correlation to Pt–Pt internuclear distances [132, 133]. Representative examples are $[\{Pt(CO)_3\}_2]^{2+}$,

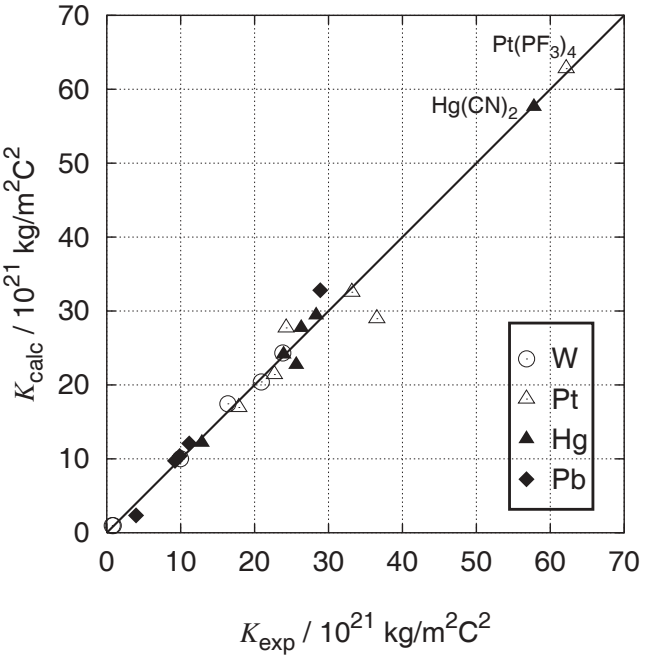


Figure 7: One-bond metal-ligand reduced nuclear spin–spin coupling constants (absolute values) for 5d metal complexes. Scalar relativistic ZORA DFT results (VWN functional) versus experimental values. A few data points for Pb are also included. Data taken from Refs. 123 and 45. The line is not a fit but indicates where $K_{calc} = K_{exp}$. The different markers indicate the different metals. For not octahedrally or tetrahedrally coordinated metal centers, the first coordination shell has been completed with solvent molecules, as described in Ref. 124

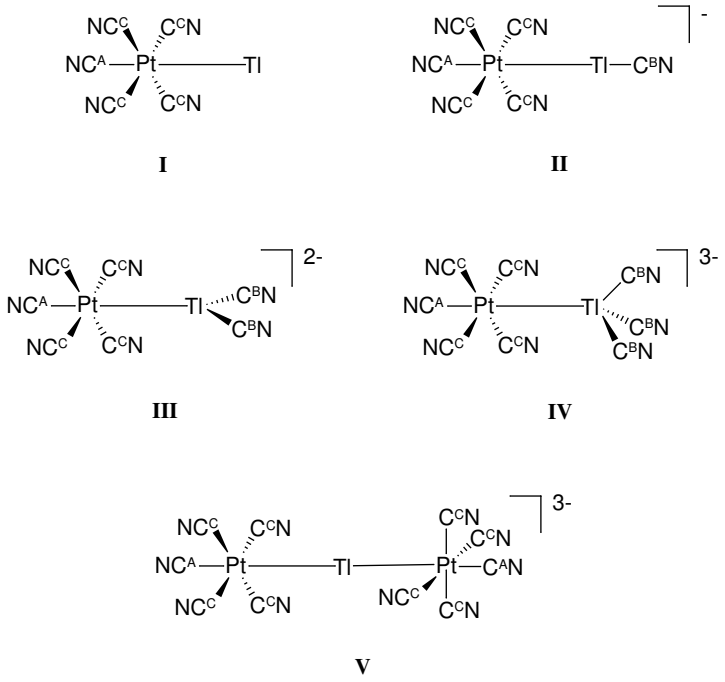


Figure 8: Structures of complexes **I**–**V**. See text for details

$[\{PtCl(CO)(PPh_3)\}_2]$ and $[\{Pt(CNCH_3)_3\}_2]^{2+}$, with small Pt-Pt coupling constants of 551, 760 and 507 Hz, respectively, and on the other hand $[\{PtCl_2(CO)\}_2]^{2-}$ and $[\{PtBr_2(CO)\}_2]^{2-}$, with large Pt-Pt coupling constants of 5250 and 4770 Hz, respectively. ZORA DFT (VWN local non–hybrid functional) computations could reproduce this order–of–magnitude difference for the systems $[Pt_2(CO)_6]^{2+}$ and $[Pt_2(CO)_2Cl_4]^{2-}$. An analysis revealed that solvent effects are not responsible for these trends, but that it is caused by the different strength of the $\sigma$ interaction of the ligands CO and $Cl^-$ with the metal–metal fragment. A simple argument based on Hückel theory shows why a stronger interaction, in particular in axial position, causes a reduction of the magnitude of $J$(Pt–Pt). The trend is greatly amplified by relativistic effects, resulting in the mentioned difference by an order of magnitude.

In Ref. 134 the extremely large coupling constants between $^{199}$Hg centers in complexes containing $Hg_2^{2+}$ and $Hg_3^{2+}$ have been investigated. It was found that consideration of *coordination* and *polarization* of a metal-metal fragment can rationalize the magnitude of the metal-metal coupling constants. The coordination can thereby be due to ligands or solvent molecules. Unlike some previously studied systems in which only one metal center could be coordinated by the solvent [124,125], solvent (or ligand) coordination of both metals of a metal-metal fragment reduces its coupling constant. A strongly polarized metal–metal bond also exhibits smaller couplings. Both effects could be rationalized by intuitive arguments based on Hückel theory [134]. For the complex of $Hg_2^{2+}$ with the crown ethers 18-crown-6 and 15-crown-5, very good agreement with the experimental $^1J$(Hg-Hg) of 284 kHz ($^{199}$Hg) [135] could be achieved. This is the currently largest experimentally determined coupling

constant. The calculated scalar DFT-ZORA result is 278 kHz (VWN local non–hybrid functional), missing SO corrections were estimated to be of the order of $-10\%$ or smaller. At the same time, the coupling constants of the (hypothetical) free $Hg_2^{2+}$ is likely to be around 0.9 MHz, indicating that an upper limit for Hg-Hg coupling constants has not yet been reached. However, a system such as the $Hg_2^{2+}$(18-crown-6)$_2$ complex for which a coupling constant of 0.6 MHz was computationally predicted does not allow an easy NMR detection of $J$(Hg-Hg) due to its symmetry. A polarization of the $Hg_2^{2+}$ fragment due to an unsymmetric environment would likely cause a reduction of the coupling, though.

In the same work [134] the one-bond and the two-bond Hg-Hg coupling constants in $Hg_3^{2+}$ have been calculated. $^2J$(Hg-Hg) has been estimated to be much larger than the one-bond coupling. Qualitatively, simple Hückel theory as well as REX (relativistic extended Hückel) calculations [136, 137] also suggest that $^2J$(Hg–Hg) $> {}^1J$(Hg–Hg). Again, environmental effects, here from the solvent $SO_2$ included in the DFT calculations, were found to be very pronounced, thus the ratio $^2J/{}^1J$ could not

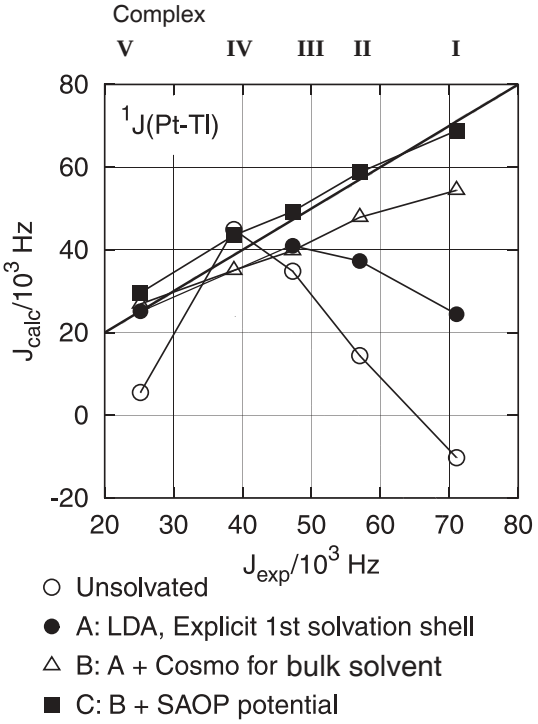


Figure 9: Nuclear spin–spin coupling constants $J(^{195}\text{Pt}–^{205}\text{Tl})$ for complexes **I** – **V** (see Fig. 8), from ZORA DFT computations. Data taken from Autschbach and Le Guennic, Ref. 126. Different computational models have been applied: Model A includes explicit water molecules (model A). In Model B, a continuum model is applied in addition to the explicit solvent molecules of Model A. Model C differs from Model B in that instead of the VWN functional the SAOP XC potential has been used which allows more accurate computations of NMR parameters [32]. The NMR measurements were carried out in aqueous solution [99, 130]

yet be predicted with confidence. In such and probably many other metal-metal bonded systems relativistic effects on spin-spin coupling constants serve as a strong "magnifying glass" for the study of the influence of coordination and solvation on the metal-metal bond.

### 4.5 Miscellaneous applications: Nuclear–independent chemical shifts (NICS) and spin–spin coupling pathways

The expression for the nuclear shielding tensor $\boldsymbol{\sigma}_A$ does not depend on any particular value of $\boldsymbol{\mu}_A$. Though the spin magnetic moment of the nucleus must not be zero in order for magnetic resonance to occur at all in an experiment, in the theoretical formalism the nuclear shielding can be calculated anyway. In consequence, an explicit expression for $\boldsymbol{\sigma}_A$ depends only on the position of the nucleus in the molecule. A quantity which has the same formula as the shielding constant can thus be calculated anywhere in space and has been named "nuclear independent chemical shift" (NICS). The NICS has been extensively applied to the question whether a given system is aromatic. The reader is referred to Vol. 101 of Chem. Rev. for an exhaustive account of aromaticity, in particular regarding various aromaticity criteria [138,139] and the concept of "ring currents" [140]. Applications to organometallic systems have been carried out. For example, it is known from experiment that the proton chemical shifts in $\eta^6$-$(C_6H_6)Cr(CO)_3$ (complex **VI**) are about 2 ppm smaller than for benzene, arousing the question whether the benzene moiety in the complex is less aromatic. This idea got strong support from a computational study of the magnetic susceptibility exaltation (MSE) of the complex as well as aromatic stabilization energies (ASE) based on an increment system [141]. It was shown that both criteria indicated a system which is less aromatic than benzene. However, an experimental NMR study from another group had earlier concluded that the complexation of benzene by $Cr(CO)_3$ increases its aromaticity [142]. The supposedly conclusive answer has finally been given by Schleyer et al. [143], who calculated NICS, ASE and MSE values for **VI** and related complexes and found that the NICS criterion for **VI** indicated a strongly aromatic system. A re–analysis of the procedure in Ref. 141 was further able to reconcile the various criteria for **VI**. It was concluded that the aromaticity of the benzene moiety in the Cr complex is similar to free benzene.

Concepts of a type that could be named "NISC" (nuclear independent spin–spin coupling) have to the best of the author's knowledge not yet been proposed. However, recently a number of publications have appeared where "nuclear spin–spin coupling densities" have been employed, for instance to study pathways of transfer of spin–polarization in small molecules [144–146]. It can be expected that such tools will soon be applied to analyze spin–spin coupling tensors in transition metal complexes.

## 5 Summary

The calculation of NMR parameters consistently requires the best computational model that is available. However, compromises have to be made regarding the computational efficiency of various methodologies, in order to make the calculations affordable. For transition metal complexes, the current method of choice is DFT, if necessary including relativistic effects. A number of program codes are available to carry out such computations in an efficient manner, which has lead to a large body of available computational data and analyses and interpretations based on these.

## Acknowledgments

The author is indebted to M. Bühl, M. Kaupp, P. Pyykkö and G. Schreckenbach who have provided him with unpublished data, preprints of upcoming articles and/or electronic files for some of the figures.

## References

[1] Kaupp, M.; Malkin, V. G.; Malkina, O. L., 'NMR of transition metal compounds', in von Ragué Schleyer, P. (editor), 'Encyclopedia of Computational Chemistry', John Wiley & Sons, Chichester, **1998**, 1857–1866.

[2] Schreckenbach, G.; Ziegler, T., 'Density functional calculations of NMR chemical shifts and ESR g-tensors', *Theor. Chem. Acc.* **1998**, *99*, 71–82.

[3] Bühl, M.; Kaupp, M.; Malkina, O. L.; Malkin, V. G., 'The DFT route to NMR chemical shifts', *J. Comput. Chem.* **1999**, *20*, 91–105.

[4] Autschbach, J.; Ziegler, T., 'Double perturbation theory: A powerful tool in computational coordination chemistry', *Coord. Chem. Rev.* **2003**, *238/239*, 83–126.

[5] Bühl, M., 'NMR of transition metal compounds', in Kaupp, M.; Bühl, M.; Malkin, V. G. (editors), 'Calculation of NMR and EPR Parameters. Theory and Applications', Wiley-VCH, Weinheim, **2004**, 421–431.

[6] Autschbach, J.; Ziegler, T., 'Relativistic Computation of NMR shieldings and Spin-spin Coupling Constants', in Grant, D. M.; Harris, R. K. (editors), 'Encyclopedia of Nuclear Magnetic Resonance', volume 9, John Wiley & Sons, Chichester, **2002**, 306–323.

[7] Autschbach, J., 'Calculation of heavy-nucleus chemical shifts: Relativistic all-electron methods', in Kaupp, M.; Bühl, M.; Malkin, V. G. (editors), 'Calculation of NMR and EPR Parameters. Theory and Applications', Wiley-VCH, Weinheim, **2004**.

[8] Autschbach, J.; Ziegler, T., 'Relativistic calculation of spin-spin coupling constants', in Kaupp, M.; Bühl, M.; Malkin, V. G. (editors), 'Calculation of NMR and EPR Parameters. Theory and Applications', Wiley-VCH, Weinheim, **2004**.

[9] Kaupp, M., 'Relativistic effects on NMR chemical shifts', in Schwerdtfeger, P. (editor), 'Relativistic electronic structure theory', volume 2, Elsevier, Amsterdam., in press.

[10] Moon, S.; Patchkovskii, S., 'First–principles calculations of paramagnetic NMR shifts', in Kaupp, M.; Bühl, M.; Malkin, V. G. (editors), 'Calculation of NMR and EPR Parameters. Theory and Applications', Wiley-VCH, Weinheim, **2004**, 325–338.

[11] Ruud, K.; Frediani, L.; Cammi, R.; Mennucci, B., 'Solvent effects on the indirect spin-spin coupling constants of benzene: The DFT-PCM approach', *Int. J. Mol. Sci.* **2003**, *4*, 119–134.

[12] Bühl, M., 'Structure, dynamics, and magnetic shieldings of permanganate ion in aqueous solution. A density functional study', *J. Phys. Chem. A* **2002**, *106*, 10505–10509.

[13] Bühl, M.; Mauschick, F. T., 'Thermal and solvent effects on $^{57}$Fe NMR chemical shifts', *Phys. Chem. Chem. Phys.* **2002**, *4*, 5508–5514.

[14] Bühl, M.; Mauschick, F. T.; Terstegen, F.; Wrackmeyer, B., 'Remarkably large geometry dependence of $^{57}$Fe NMR chemical shifts', *Angew. Chem. Int. Ed.* **2002**, *41*, 2312–2315.

[15] Wasylishen, R., 'Dipolar and Indirect Coupling Tensors in Solids', in Grant, D. M.; Harris, R. K. (editors), 'Encyclopedia of Nuclear Magnetic Resonance', John Wiley & Sons, **1996**, 1685–1695.

[16] Wasylishen, R., 'Characterization of NMR tensors via experiment and theory', in Kaupp, M.; Bühl, M.; Malkin, V. G. (editors), 'Calculation of NMR and EPR Parameters. Theory and Applications', Wiley-VCH, Weinheim, **2004**, 433–447.

[17] Gauss, J., 'Molecular Properties', in Grotendorst, J. (editor), 'Modern methods and algorithms of quantum chemistry', volume 3 of *NIC*, John von Neumann Institute for Computing, Jülich, **2000**, 541–592.

[18] Epstein, S. T., *The Variation Method in Quantum Chemistry*, Academic Press, New York, **1974**.

[19] Helgaker, T.; Jaszuński, M.; Ruud, K., 'Ab initio methods for the calculation of NMR shielding and indirect spin-spin coupling constants', *Chem. Rev.* **1999**, *99*, 293–352.

[20] Helgaker, T.; Pecul, M., 'Spin–spin coupling constants with HF and DFT methods', in Kaupp, M.; Bühl, M.; Malkin, V. G. (editors), 'Calculation of NMR and EPR Parameters. Theory and Applications', Wiley-VCH, Weinheim, **2004**, 101–121.

[21] Fleischer, U.; van Wüllen, C.; Kutzelnigg, W., 'NMR Chemical Shift Computation: Ab Initio', in von Ragué Schleyer, P. (editor), 'Encyclopedia of Computational Chemistry', John Wiley & Sons, Chichester, **1998**, 1827–1835.

[22] McWeeny, R., *Methods of molecular quantum mechanics*, Academic Press, London, 2nd edition, **1992**.

[23] Hellmann, H., 'Zur Rolle der kinetischen Elektronenenergie für die zwischenatomaren Kräfte', *Z. Phys.* **1933**, *85*, 180–190.

[24] Nakatsuji, H.; Sugimoto, M.; Saito, S., 'Electronic origin of $^{95}$ Mo NMR chemical shifts in molybdenum complexes. Relationship between excitation energy and chemical shift.', *Inorg. Chem.* **1990**, *29*, 3095–3097.

[25] Lee, A. M.; Handy, N. C.; Colwell, S. M., 'The density functional calculation of nuclear shielding constants using London atomic orbitals', *J. Chem. Phys.* **1995**, *103*, 10095–10109.

[26] Malkin, V. G.; Malkina, O. L.; Salahub, D. R., 'Calculations of NMR shielding constants beyond uncoupled density functional theory. IGLO approach', *Chem. Phys. Lett.* **1993**, *204*, 87–95.

[27] Malkin, V. G.; Malkina, O. L.; Eriksson, L. A.; Salahub, D. R., 'The calculation of NMR and ESR spectroscopy parameters using density functional theory', in Seminario, J. M.; Politzer, P. (editors), 'Modern Density Functional Theory: A Tool for Chemistry', volume 2, Elsevier, **1995**, 273–347.

[28] Fadda, E.; Casida, M. E.; Salahub, D. R., 'Time–dependent density functional theory as a foundation for a firmer understanding of sum–over–states density functional perturbation theory: "Loc.3" approximation', *Int. J. Quantum Chem.* **2003**, *91*, 67–83.

[29] Fadda, E.; Casida, M. E.; Salahub, D. R., 'NMR shieldings from sum–over–states density–functional–perturbation theory: Further testing of the "Loc.3" approximation', *J. Chem. Phys.* **2003**, *118*, 6758–6768.

[30] Patchkovskii, S.; Autschbach, J.; Ziegler, T., 'Curing difficult cases in magnetic properties prediction with self-interaction corrected density functional theory', *J. Chem. Phys.* **2001**, *115*, 26–42.

[31] Patchkovskii, S.; Ziegler, T., 'Phosphorus NMR chemical shifts with self–interaction free, gradient–corrected DFT', *J. Phys. Chem. A* **2002**, *106*, 1088–1099.

[32] Poater, J.; van Lenthe, E.; Baerends, E. J., 'Nuclear magnetic resonance chemical shifts with the statistical average of orbital-dependent model potential in Kohn-Sham density functional theory', *J. Chem. Phys.* **2003**, *118*, 8584–8593.

[33] Nomura, Y.; Takeuchi, Y.; Nakagawa, N., 'Substituent effects in aromatic proton NMR spectra. III. Substituent effects caused by halogens', *Tetrahedron Lett.* **1969**, *8*, 639–642.

[34] Morishima, I.; Endo, K.; Yonezawa, T., 'Effect of the heavy atom on the nuclear shielding constant. I. The proton chemical shifts in hydrogen halides', *J. Chem. Phys.* **1973**, *59*, 3356–3364.

[35] Kaupp, M.; Malkina, O. L.; Malkin, V. G.; Pyykkö, P., 'How do spin-orbit induced heavy atom effects on NMR chemical shifts function? Validation of a simple analogy to spin-spin coupling by density functional theory (DFT) calculations on some Iodo compounds', *Chem. Eur. J.* **1998**, *4*, 118–126.

[36] Almlöf, J.; Gropen, O., 'Relativistic effects in chemistry', in Lipkowitz, K. B.; Boyd, D. B. (editors), 'Reviews in computational chemistry', volume 8, VCH Publishers Inc., New York, **1996**, 203–244.

[37] Pyykkö, P., 'Relativistic Effects in Structural Chemistry', *Chem. Rev.* **1988**, *88*, 563–594.

[38] Moss, R. E., *Advanced Molecular Quantum Mechanics*, Chapman and Hall, London, **1973**.

[39] Sadlej, A. J., 'Methods of relativistic quantum chemistry', in Roos, B. O. (editor), 'Lecture Notes in Chemistry II', volume 64 of *Lecture notes in chemistry*, Springer, Berlin, **1994**, 203–230.

[40] Hess, B. A., 'Relativistic theory and applications', in von Ragué Schleyer, P. (editor), 'Encyclopedia of computational chemistry', John Wiley & Sons, Chichester, **1998**, 2499–2508.

[41] van Lenthe, E.; Baerends, E. J.; Snijders, J. G., 'Relativistic regular two-component Hamiltonians', *J. Chem. Phys.* **1993**, *99*, 4597–4610.

[42] van Lenthe, E., *The ZORA Equation*, Ph.D. thesis, Vrije Universiteit Amsterdam, Netherlands, **1996**.

[43] Wolff, S. K.; Ziegler, T.; van Lenthe, E.; Baerends, E. J., 'Density functional calculations of nuclear magnetic shieldings using the zeroth-order regular approximation (ZORA) for relativistic effects: ZORA nuclear magnetic resonance', *J. Chem. Phys.* **1999**, *110*, 7689–7698.

[44] Bouten, R.; Baerends, E. J.; van Lenthe, E.; Visscher, L.; Schreckenbach, G.; Ziegler, T., 'Relativistic effects for NMR shielding constants in transition metal oxides using the zeroth-order regular approximation', *J. Chem. Phys.* **2000**, *104*, 5600–5611.

[45] Autschbach, J.; Ziegler, T., 'Nuclear spin-spin coupling constants from regular approximate relativistic density functional calculations. I. Formalism and scalar relativistic results for heavy metal compounds', *J. Chem. Phys.* **2000**, *113*, 936–947.

[46] Autschbach, J.; Ziegler, T., 'Nuclear spin-spin coupling constants from regular approximate relativistic density functional calculations. II. Spin-orbit coupling effects and anisotropies', *J. Chem. Phys.* **2000**, *113*, 9410–9418.

[47] Fukuda, R.; Hada, M.; Nakatsuji, H., 'Quasirelativistic theory for the magnetic shielding constant. I. Formulation of Douglas-Kroll-Hess transformation for the magnetic field and its application to atomic systems', *J. Chem. Phys.* **2003**, *118*, 1015–1026.

[48] Fukuda, R.; Hada, M.; Nakatsuji, H., 'Quasirelativistic theory for magnetic shielding constants. II. Gauge-including atomic orbitals and applications to molecules', *J. Chem. Phys.* **2003**, *118*, 1027–1035.

[49] Fukui, H.; Baba, T., 'Calculation of nuclear magnetic shieldings. XV. Ab initio zeroth-order regular approximation method', *J. Chem. Phys.* **2002**, *117*, 7836–7844.

[50] Baba, T.; Fukui, H., 'Calculation of nuclear magnetic shieldings. XIV. Relativistic mass-velocity corrected perturbation Hamiltonians', *Mol. Phys.* **2002**, *100*, 623–633.

[51] Schreckenbach, G.; Ziegler, T., 'Calculation of NMR shielding tensors based on density functional theory and a scalar relativistic Pauli-type Hamiltonian. The application to transition metal complexes', *Int. J. Quantum Chem.* **1997**, *61*, 899–918.

[52] Wolff, S. K.; Ziegler, T., 'Calculation of DFT-GIAO NMR shifts with the inclusion of spin-orbit coupling', *J. Chem. Phys.* **1998**, *109*, 895–905.

[53] Khandogin, J.; Ziegler, T., 'A simple relativistic correction to the nuclear spin-spin coupling constant', *J. Phys. Chem. A* **2000**, *104*, 113–120.

[54] Schwerdtfeger, P.; Brown, J. R.; Laerdahl, J. K.; Stoll, H., 'The accuracy of the pseudopotential approximation. III. A comparison between pseudopotential and all-electron methods for Au and AuH pseudopotential and all-electron methods for Au and AuH', *J. Chem. Phys.* **2000**, *113*, 7110–7118.

[55] Pyykkö, P., 'Theory of NMR parameters. From Ramsey to relativity, 1953 to 1983', in Kaupp, M.; Bühl, M.; Malkin, V. G. (editors), 'Calculation of NMR and EPR Parameters. Theory and Applications', Wiley-VCH, Weinheim, **2004**, 7–19.

[56] Ballhausen, C. J., *Molecular Electronic Structures of Transition Metal Complexes*, McGraw-Hill, London, **1979**.

[57] De Brouckere, G., 'Calculation of observables in metallic complexes by the molecular orbital theory', *Adv. Chem. Phys.* **1978**, *37*, 203–304.

[58] Tossell, J. A. (Editor), *Nuclear Magnetic Shieldings and Molecular Structure*, Kluwer, Dordrecht, **1993**.

[59] Bieger, W.; Seifert, G.; Eschrig, H.; Grossmann, G., 'LCAO X$\alpha$ calculations of nuclear magnetic shielding in molecules', *Chem. Phys. Lett.* **1985**, *115*, 275–280.

[60] Freier, D. G.; Fenske, R. F.; Xiao-Zheng, Y., 'Theoretical calculations of carbon–13 NMR chemical shifts via the X$\alpha$ scattered wave method', *J. Chem. Phys.* **1985**, *83*, 3526–3537.

[61] Malkin, V. G.; Zhidomirov, G. M., 'SCF-X$\alpha$-DV calculations of the nuclear magnetic shielding tensor', *Zh. Strukt. Khim.* **1988**, *29*, 32–36.

[62] Kaupp, M.; Malkina, O. L.; Malkin, V. G., 'The calculation of $^{17}$O chemical shielding in transition metal oxo complexes. I. Comparison of DFT an ab initio approaches, and mechanism of relativity-induced shielding', *J. Chem. Phys.* **1997**, *106*, 9201–9212.

[63] Malkin, V. G.; Malkina, O. L.; Salahub, D. R., 'Calculations of NMR shielding constants by uncoupled density functional theory', *Chem. Phys. Lett.* **1993**, *204*, 80–86.

[64] Arduengo, A. J.; Dixon, D. A.; Kumashiro, K. K.; Lee, C.; Power, W. P.; Zilm, K. W., 'Chemical shielding tensor of a carbene', *J. Am. Chem. Soc.* **1994**, *116*, 6361–6367.

[65] Schreckenbach, G.; Ziegler, T., 'Calculation of NMR shielding tensors using gauge-including atomic orbitals and modern density functional theory', *J. Phys. Chem.* **1995**, *99*, 606–611.

[66] Rauhut, G.; Puyear, S.; Wolinski, K.; Pulay, P., 'Comparison of NMR shieldings calculated from Hartree–Fock and density functional wave functions using gauge–including atomic orbitals', *J. Phys. Chem.* **1996**, *100*, 6310–6316.

[67] Cheeseman, J. R.; Trucks, G. W.; Keith, T. A.; Frisch, M. J., 'A comparison of models for calculating nuclear magnetic resonance shielding tensors', *J. Chem. Phys.* **1996**, *104*, 5497–5509.

[68] Malkin, V. G.; Malkina, O. L.; Salahub, D. R., 'Calculation of spin–spin coupling constants using density functional theory', *Chem. Phys. Lett.* **1994**, *221*, 91–99.

[69] Dickson, R. M.; Ziegler, T., 'NMR spin–spin coupling constants from density functional theory with Slater–type basis functions', *J. Phys. Chem.* **1996**, *100*, 5286–5290.

[70] Helgaker, T.; Watson, M.; Handy, N. C., 'Analytical calculation of nuclear magnetic resonance indirect spin-spin coupling constants at the generalized gradient approximation and hybrid levels of theory', *J. Chem. Phys.* **2000**, *113*, 9402–9409.

[71] Sychrovský, V.; Gräfenstein, J.; Cremer, D., 'Nuclear magnetic resonance spin-spin coupling constants from coupled perturbed density functional theory', *J. Chem. Phys.* **2000**, *113*, 3530–3547.

[72] Breit, G., 'Possible effects of nuclear spin on X-ray terms', *Phys. Rev.* **1930**, *35*, 1447–1451.

[73] Kaupp, M.; Malkin, V. G.; Malkina, O. L.; Salahub, D. R., 'Scalar relativistic effects on $^{17}$O NMR chemical shifts in transition-metal oxo complexes. An ab initio ECP/DFT study', *J. Am. Chem. Soc.* **1995**, *117*, 1851–1852, erratum *ibid.*, p. 8492.

[74] Kaupp, M.; Malkin, V. G.; Malkina, O. L.; Salahub, D. R., 'Calculation of ligand NMR chemical shifts in transition metal complexes using ab-initio effective core potentials and density functional theory', *Chem. Phys. Lett.* **1995**, *235*, 382–388.

[75] Visscher, L.; Enevoldsen, T.; Saue, T.; Jensen, H. J. A.; Oddershede, J., 'Full four-component relativistic calculations of NMR shieldings and indirect spin-spin coupling tensors in hydrogen halides', *J. Comput. Chem.* **1999**, *20*, 1262–1273.

[76] Enevoldsen, T.; Visscher, L.; Saue, T.; Jensen, H. J. A.; Oddershede, J., 'Relativistic four-component calculations of indirect nuclear spin-spin couplings in $MH_4$ (M=C, Si, Ge, Sn, Pb) and $Pb(CH_3)H$', *J. Chem. Phys.* **2000**, *112*, 3493–3498.

[77] Malkin, V. G.; Malkina, O. L.; Salahub, D. R., 'Spin-orbit corrections to NMR shielding constants from density functional theory', *Chem. Phys. Lett.* **1996**, *261*, 335–345.

[78] Malkina, O. L.; Schimmelpfennig, B.; Kaupp, M.; Hess, B. A.; Chandra, P.; Wahlgren, U.; Malkin, V. G., 'Spin-orbit corrections to NMR shielding constants from density functional theory. How important are the two-electron terms?', *Chem. Phys. Lett.* **1998**, *296*, 93–104.

[79] Vaara, J.; Malkina, O. L.; Stoll, H.; Malkin, V. G.; Kaupp, M., 'Study of relativistic effects on nuclear shieldings using density functional theory and spin-orbit pseudopotentials', *J. Chem. Phys.* **2001**, *114*, 61–71.

[80] Koch, W.; Holthausen, M. C., *A Chemist's Guide to Density Functional Theory*, Wiley-VCH, Weinheim, **2001**.

[81] Ruiz-Morales, Y.; Schreckenbach, G.; Ziegler, T., 'Origin of the hydrydic $^{1}$H chemical shift in low–valent transition metal hydrides', *Organometallics* **1996**, *15*, 3920–3923.

[82] Ehlers, A. W.; Ruiz-Morales, Y.; Baerends, E. J.; Ziegler, T., 'Dissociation enrgies, vibrational frequencies and $^{13}$C NMR chemical shifts of the 18-electron species $[M(CO)_6]^n$ (M = Hf-Ir, Mo, Tc, Ru, Cr, Mn, Fe). A density functional study', *Inorg. Chem.* **1997**, *36*, 5031–5036.

[83] Ruiz-Morales, Y.; Schreckenbach, G.; Ziegler, T., 'Theoretical study of $^{13}$C and $^{17}$O NMR shielding tensors in transition metal carbonyls based on density functional theory and gauge-including atomic orbitals', *J. Phys. Chem.* **1996**, *100*, 3359–3367.

[84] Lammertsma, K., 'Phosphinidenes', *Top. Curr. Chem.* **2003**, *229*, 95–119.

[85] Termaten, A. J.; Aktas, H.; Schakel, M.; Ehlers, A. W.; Lutz, M.; Spek, A. L.; Lammertsma, K., 'Terminal phosphinidene complexes Cp*(L)M=PAr of the group 9 transition metals cobalt, rhodium, and iridium. Synthesis, structures, and properties', *Organometallics* **2003**, *22*, 1827–1834.

[86] Webster, C. E.; Hall, M. B., 'Factors affecting the structure of substituted tris(pyrazolyl)borate rhodium dicarbonyl complexes', *Inorg. Chim. Acta* **2002**, *330*, 268–282.

[87] Wagener, T.; Frenking, G., 'Theoretical study of transition metal compounds with molybdenum– and tungsten–phosphorus triple bonds', *Inorg. Chem.* **1998**, *37*, 1805–1811.

[88] Zurek, E.; Ziegler, T., 'Toward the Identification of Dormant and Active Species in MAO (Methylaluminoxane)-Activated, Dimethylzirconocene-Catalyzed Olefin Polymerization', *Organometallics* **2002**, *21*, 83–92.

[89] Gracia, J.; Martín, A.; Mena, M.; del Carmen Morales-Varela, M.; Poblet, J.-M.; Santamaría, C., 'Intercalation of alkali metal cations into layered organolithium oxides', *Angew. Chem. Int. Ed.* **2003**, *42*, 927–930.

[90] Strohmeier, M.; Ohrendt, A. M.; Facelli, J. C.; Solum, M. S.; Pugmire, R. J.; Parry, R. W.; Grant, D. M., 'Solid state $^{15}$N and $^{13}$C NMR study of several metal 5,10,15,20–Tetraphenylporphyrin systems', *J. Am. Chem. Soc.* **1997**, *119*, 7114–7120.

[91] McMahon, M. T.; deDios, A. C.; Godbout, N.; Salzmann, R.; Laws, D. D.; Le, H.; Havlin, R. H.; Oldfield, E., 'An Experimental and Quantum Chemical Investigation of CO Binding to Heme Proteins and Model Systems: A Unified Model Based on $^{13}$C, $^{17}$O, and $^{57}$Fe Nuclear Magnetic Resonance and $^{57}$Fe Mössbauer and Infrared Spectroscopies', *J. Am. Chem. Soc.* **1998**, *120*, 4784–4797.

[92] Schreckenbach, G.; Wolff, S. K.; Ziegler, T., 'Covering the entire periodic table: Relativistic density functional calculations of NMR chemical shifts in diamagnetic actinide compounds', in Facelli, J. C.; de Dios, A. C. (editors), 'Modeling NMR chemical shifts', Number 732 in ACS Symposium Series, American Chemical Society, Boston, Mass., **1999**, 101–114.

[93] Schreckenbach, G.; Wolff, S. K.; Ziegler, T., 'NMR shielding calculations across the Periodic Table: Diamagnetic Uranium compounds. 1. Methods and issues', *J. Phys. Chem. A* **2000**, *104*, 8244–8255.

[94] Schreckenbach, G., 'On the relation between a common gauge origin formulation and the GIAO formulation of the NMR shielding tensor', *Theor. Chem. Acc.* **2002**, *108*, 246–253.

[95] Schreckenbach, G., 'Density functional calculations of $^{19}$F and $^{235}$U NMR chemical shifts in uranium (VI) chloride fluorides $UF_{6-n}Cl_n$: The influence of the relativistic approximation and the role of the exchange–correlation functional', *Int. J. Quantum Chem.* **2003**, submitted for publication.

[96] Bühl, M.; Mauschick, F. T.; Schurhammer, R., 'Theoretical studies of structures of vanadate complexes in aqueous solution', in Wagner, S.; Handke, W.; Bode, A.; Durst, F. (editors), 'High Performance Computing in Science and Engineering, Munich 2002', Springer, Berlin, **2003**, 189–199.

[97] Kaupp, M., 'Habilitationsschrift', **1996**.

[98] Lichtenberger, D. L., 'Electron distribution, bonding, and $J$(Si–H) NMR coupling constant in ($\eta^5$–$C_5H_5$)$(CO)_2$MnHSi$Cl_3$: The molecular orbital view', *Organometallics* **2003**, *22*, 1599–1602.

[99] Maliarik, M.; Berg, K.; Glaser, J.; Sandström, M.; Tóth, I., 'New class of oligonuclear Platinum-Thallium compounds with a direct metal–metal bond. 2. Structural characterization of the complexes', *Inorg. Chem.* **1998**, *37*, 2910–2919.

[100] Bacskay, G. B.; Bytheway, I.; Hush, N. S., 'H-D spin-spin coupling in stretched molecular hydrogen complexes of osmium(II): Density functional studies of $J_{HD}$', *J. Am. Chem. Soc.* **1996**, *118*, 3753–3756.

[101] Craw, J. S.; Bacskay, G. B.; Hush, N. S., 'Stretched molecular hydrogen complexes of Osmium(II): A quantum chemical study of the influence of the trans ligand on geometries, spin–spin coupling constants, bonding, and charge distributions', *J. Am. Chem. Soc.* **1994**, *116*, 5937–5948.

[102] Bühl, M., 'Density functional computations of transition metal NMR chemical shifts: Dramatic effects of Hartree–Fock exchange', *Chem. Phys. Lett.* **1997**, *267*, 251–257.

[103] Bühl, M., 'Density functional calculations of $^{95}$Mo chemical shifts: applications to model catalysts for imine metathesis', *Chem. Eur. J.* **1999**, *5*, 3514–3522.

[104] Nakatsuji, H.; Hu, Z.-M.; Nakajima, T., 'Spin-orbit effect on the magnetic shielding constant: Niobium hexahilades and titanium tetrahalides', *Chem. Phys. Lett.* **1997**, *275*, 429–436.

[105] Bühl, M., 'Density functional computation of $^{55}$Mn NMR parameters', *Theor. Chem. Acc.* **2002**, *107*, 336–342.

[106] Chan, J. C. C.; Au-Yeung, C. F., 'Density functional study of $^{59}$Co chemical shielding tensors using gauge–including atomic orbitals', *J. Phys. Chem. A* **1997**, *101*, 3637–3640.

[107] Godbout, N.; Oldfield, E., 'Density functional study of cobalt–59 nuclear magnetic resonance chemical shifts and shielding tensor elements in Co(III) complexes', *J. Am. Chem. Soc.* **1997**, *119*, 8065–8069.

[108] Bühl, M.; Hamprecht, F. A., 'Theoretical investigations of NMR chemical shifts and reactivities of oxovanadium(V) compounds', *J. Comput. Chem.* **1998**, *19*, 113–122.

[109] Kidambi, S. S.; Ramamoorthy, A., 'Characterization of metal centers in bioinorganic complexes using ab initio calculations of $^{113}$Cd chemical shifts', *Inorg. Chem.* **2003**, *42*, 2200–2202.

[110] Kidambi, S. S.; Lee, D.-K.; Ramamoorthy, A., 'Interaction of Cd and Zn with biologically important ligands characterized using solid–state NMR and ab–initio calculations', *Inorg. Chem.* **2003**, *42*, 3142–3151.

[111] Krauss, M.; Olsen, L.; Antony, J.; Hemmingsen, L., 'Coordination geometries of Zn(II) and Cd(II) in phosphotriesterase: Influence of water molecules in the active site', *J. Phys. Chem. B* **2002**, *106*, 9446–9453.

[112] Edlund, U.; Lejon, T.; Pyykkö, P.; Venkatachalam, T. K.; Buncel, E., '$^{7}$Li, $^{29}$Si, $^{119}$Sn, and $^{207}$Pb NMR studies of phenyl-substituted group 4 anions', *J. Am. Chem. Soc.* **1987**, *109*, 5982–5985.

[113] Rodriguez-Fortea, A.; Alemany, P.; Ziegler, T., 'Density functional calculations of NMR chemical shifts with the inclusion of spin-orbit coupling in tungsten and lead compounds', *J. Phys. Chem. A* **1999**, *103*, 8288–8294.

[114] Hada, M.; Kaneko, H.; Nakatsuji, H., 'Relativistic study of nuclear magnetic shielding constants: Tungsten hexahalides and tetraoxide', *Chem. Phys. Lett.* **1996**, *261*, 7–12.

[115] Autschbach, J.; Hess, B. A.; Johansson, P. A.; Neugebauer, J.; Patzschke, M.; Pyykkö, P.; Reiher, M.; Sundholm, D., 'Properties of $WAu_{12}$', *Phys. Chem. Chem. Phys.* **2004**, *6*, 11–22.

[116] Gilbert, T. M.; Ziegler, T., 'Prediction of $^{195}$Pt NMR chemical shifts by density functional theory computations: the importance of magnetic coupling and relativistic effects in explaining trends', *J. Phys. Chem. A* **1999**, *103*, 7535–7543.

[117] Bühl, M.; Parrinello, M., 'Medium effects on $^{51}$V NMR chemical shifts: A density functional study', *Chem. Eur. J.* **2001**, *7*, 4487–4494.

[118] Marx, D.; Hutter, J., 'Ab initio molecular dynamics: Theory and implementation', in Grotendorst, J. (editor), 'Modern methods and algorithms of quantum chemistry', volume 3 of *NIC*, John von Neumann Institute for Computing, Jülich, **2000**, 329–477.

[119] Khandogin, J.; Ziegler, T., 'A density functional study of nuclear magnetic resonance spin-spin coupling constants in transition metal systems', *Spectrochim. Acta* **1999**, *A 55*, 607–624.

[120] Bryce, D. L.; Wasylishen, R. E.; Autschbach, J.; Ziegler, T., 'Periodic Trends in Indirect Nuclear Spin-Spin Coupling Tensors: Relativistic Density Functional Calculations for Interhalogen Diatomics', *J. Am. Chem. Soc.* **2002**, *124*, 4894–4900.

[121] Pyykkö, P.; Pajanne, E.; Inokuti, M., 'Hydrogen-like relativistic corrections for electric and magnetic hyperfine integrals', *Int. J. Quantum Chem.* **1973**, *7*, 785–806.

[122] Pyykkö, P., 'Perspective on Norman Ramsey's theories of NMR chemical shifts and nuclear spin-spin coupling', *Theor. Chem. Acc.* **2000**, *103*, 214–216.

[123] Autschbach, J.; Ziegler, T., 'Calculating electric and magnetic properties from time dependent density functional perturbation theory', *J. Chem. Phys.* **2002**, *116*, 891–896.

[124] Autschbach, J.; Ziegler, T., 'Solvent effects on heavy atom nuclear spin-spin coupling constants: A theoretical study of Hg-C and Pt-P couplings', *J. Am. Chem. Soc.* **2001**, *123*, 3341–3349.

[125] Autschbach, J.; Ziegler, T., 'A theoretical investigation of the remarkable spin-spin coupling pattern in $[(NC)_5Pt\text{-}Tl(CN)]^-$', *J. Am. Chem. Soc.* **2001**, *123*, 5320–5324.

[126] Autschbach, J.; Le Guennic, B., 'A theoretical study of the NMR spin–spin coupling constants of the complexes $[(NC)_5Pt\text{–}Tl(CN)_n]^{n-}$ (n = 0 – 3) and $[(NC)_5Pt\text{–}Tl\text{–}Pt(CN)_5]^{3-}$: A lesson on environmental effects', *J. Am. Chem. Soc.* **2003**, *125*, 13585–13593.

[127] Klamt, A.; Schüürmann, G., 'COSMO: A new approach to dielectric screening in solvents with explicit expressions for the screening energy and its gradient', *J. Chem. Soc. Perkin Trans. 2* **1993**, 799–805.

[128] Pye, C. C.; Ziegler, T., 'An implementation of the conductor-like screening model of solvation within the Amsterdam density functional package', *Theor. Chem. Acc.* **1999**, *101*, 396–408.

[129] Schipper, P. R. T.; Gritsenko, O. V.; van Gisbergen, S. J. A.; Baerends, E. J., 'Molecular calculations of excitation energies and (hyper)polarizabilities with a statistical average of orbital model exchange-correlation potentials', *J. Chem. Phys.* **2000**, *112*, 1344–1352.

[130] Berg, K. E.; Glaser, J.; Read, M. C.; Tóth, I., 'Nonbuttressed metal–metal–bonded complexes of Platinum and Thallium in aqueous solution: Characterization of $[(NC)_5Pt\text{-}Tl(CN)]^-$ by multinuclear NMR', *J. Am. Chem. Soc.* **1995**, *117*, 7550–7751.

[131] Autschbach, J.; Igna, C. D.; Ziegler, T., 'A theoretical investigation of the apparently irregular behavior of Pt-Pt spin-spin coupling constants', *J. Am. Chem. Soc.* **2003**, *125*, 1028–1032.

[132] Boag, N. M.; Browning, J.; Crocker, C.; Goggin, P. L.; Goodfellow, R. J.; Murray, M.; Spencer, J. L., 'Effect of complex type on $^{195}Pt\text{-}^{195}Pt$ spin-spin coupling constants', *J. Chem. Res. (M)* **1978**, 2962–2990.

[133] Xu, Q.; Heaton, B. T.; Jacob, C.; Mogi, K.; Ichihashi, Y.; Souma, Y.; Kanamori, K.; Eguchi, T., 'Hexacarbonyldiplatinum(I). Synthesis, Spectroscopy, and Density Functional Calculation of the First Homoleptic, Dinuclear Diplatinum(I) Carbonyl Cation, $[\{Pt(CO)_3\}_2]^{2+}$, Formed in Concentrated Sulphuric Acid', *J. Am. Chem. Soc.* **2000**, *122*, 6862–6870.

[134] Autschbach, J.; Igna, C. D.; Ziegler, T., 'A theoretical study of the large Hg-Hg spin-spin coupling constants in $Hg_2^{2+}$, $Hg_3^{2+}$, and $Hg_2^{2+}$ – crown-ether complexes', *J. Am. Chem. Soc.* **2003**, *125*, 4937–4942.

[135] Malleier, R.; Kopacka, H.; Schuh, W.; Wurst, K.; Peringer, P., '$^1J$(199Hg-199Hg) values of up to 284 kHz in complexes of $[Hg\text{-}Hg]^{2+}$ with crown ethers: The largest indirect coupling constants', *Chem. Comm.* **2001**, 51–52.

[136] Contreras, R. H.; Facelli, J. C., 'Advances in theoretical and physical aspects of spin-spin coupling constants', *Annu. Rep. NMR Spectrosc.* **1993**, *27*, 255–356.

[137] Pyykkö, P., unpublished REX results for $Hg_3^{2+}$.

[138] Katritzky, A. R.; Jug, K.; Oniciu, D. C., 'Quantitative measures for aromaticity for mono-, bi-, and tricyclic penta- and hexaatomic heteroaromatic ring systems and their interrelationships', *Chem. Rev.* **2001**, *101*, 1421–1449.

[139] De Proft, F.; Geerlings, P., 'Conceptual and computational DFT in the study of aromaticity', *Chem. Rev.* **2001**, *101*, 1451–1464.

[140] Gomes, J. A. N. F.; Mallion, R. B., 'Aromaticity and ring currents', *Chem. Rev.* **2001**, *101*, 1349–1383.

[141] Simion, D. V.; Sorensen, T. S., 'A theoretical computation of the aromaticity of (Benzene)$Cr(CO)_3$ compared to benzene using the exaltation of magnetic susceptibility criterion and a comparison of calculated and experimental NMR chemical shifts in these compounds', *J. Am. Chem. Soc.* **1996**, *118*, 7345–7352.

[142] Mitchell, R. H.; Zhou, P.; Venugopalan, S.; Dingle, T. W., 'Synthesis of the first metal-complexed benzannulene. An estimate of the aromaticity of tricarbonylchromium-complexed benzene relative to the aromaticity of benzene itself', *J. Am. Chem. Soc.* **1990**, *112*, 7812–7813.

[143] Schleyer, P. v. R.; Kiran, B.; Simion, D. V.; Sorensen, T. S., 'Does $Co(CO)_3$ complexation reduce the aromaticity of benzene?', *J. Am. Chem. Soc.* **2000**, *122*, 510–513.

[144] Soncini, A.; Lazzeretti, P., 'Nuclear spin–spin coupling density functions and the Fermi hole', *J. Chem. Phys.* **2003**, *119*, 1343–1349.

[145] Malkina, O. L.; Malkin, V. G., 'Visualization of nuclear spin–spin coupling pathways by real–space functions', *Angew. Chem. Int. Ed.* **2003**, *42*, 4335–4338.

[146] Wu, A.; Graefenstein, J.; Cremer, D., 'Analysis of the transmission mechanism of NMR spin–spin coupling constants using Fermi contact spin density distribution, partial spin polarization, and orbital currents. $XH_n$ molecules', *J. Phys. Chem. A* **2003**, *107*, 7043–7056.